SIAM J. APPL. MATH.
Vol. 61, No. 5, pp. 1731–1761

THE MECHANICS OF LUNG TISSUE UNDER HIGH-FREQUENCY VENTILATION*

MARKUS R. OWEN†‡ AND MARK A. LEWIS†

Abstract. High-frequency ventilation is a radical departure from conventional lung ventilation, with frequencies greater than 2Hz, and volumes per breath much smaller than the anatomical dead-space. Its use has been shown to benefit premature infants and patients with severe respiratory distress, but a vital question concerns ventilator-induced damage to the lung tissue, and a clear protocol for the most effective treatment has not been identified. Mathematical modeling can help in understanding the mechanical effects of lung ventilation, and hence in establishing such a protocol.

In this paper we describe the use of homogenization theory to predict the macroscopic behavior of lung tissue based upon the three dimensional microstructure of respiratory regions, making the simplifying assumption that the microstructure is periodic. This approach yields equations for macroscopic air flow, pressure, and tissue deformation, with parameters which can be determined from a specification of the tissue microstructure and its material properties. We are able to include an alternative hypothesis as to the dependence of lung tissue shear viscosity on the frequency of forcing, known as the structural damping hypothesis.

We then show how, if we consider isotropic tissue, the parameters determining the macroscopic response of the tissue can be estimated from bulk measurements. Finally, we consider the solutions of the macroscopic system when we consider variations in just one spatial dimension. In particular, we demonstrate that the structural damping hypothesis leads to markedly different solution behavior.

Key words. biomaterials, homogenization, lung ventilation, viscoelasticity

AMS subject classifications. 76Z05, 92C10, 92C35

PII. S0036139999363652

1. Introduction.

Strategies to reduce the likelihood of lung tissue damage during mechanical ventilation include the use of high-frequency oscillation [5]. High-frequency oscillation (HFO) is a method of mechanical ventilation where small volume, high-frequency breaths (> 2Hz) are administered to the lung. This small volume-rapid rate method is a radical departure from normal respiration or conventional mechanical ventilation where large tidal volume breaths are given at low frequencies (< 0.25Hz). Despite these differences, HFO has proven beneficial to facilitating gas transfer in premature infants, children, and adults suffering from respiratory insufficiency secondary to various lung disease states.

Since the breath volumes administered in HFO are much smaller than the volume necessary to fill the lungs, the question arises as to how HFO can ventilate at all. A partial answer is given by Chang [3] and others who have analyzed the different modes of gas transport that occur during HFO. Convective dispersion of gas in the bronchi due to asymmetric flow profiles during inspiration and expiration and alveolar ventilation by out-of-phase HFO are thought to be particularly significant. The out-of-phase HFO arises from differential filling of parallel lung units that have different

*Received by the editors November 3, 1999; accepted for publication (in revised form) October 3, 2000; published electronically March 7, 2001. This research was partially supported by National Science Foundation grants DMS-9457816 (MRO and MAL) and DMS-9973212 (MAL), by the Institute for Mathematics and its Applications with funds provided by the National Science Foundation (MAL), and by a University of Utah seed grant (MRO).

http://www.siam.org/journals/siap/61-5/36365.html

†Department of Mathematics, University of Utah, Salt Lake City, UT 84112 (owen@math.utah.edu, mlewis@math.utah.edu).

‡Current address: Nonlinear and Complex Systems Group, Department of Mathematical Sciences, Loughborough University, Loughborough, LE11 3TU, UK (M.R.Owen@lboro.ac.uk).

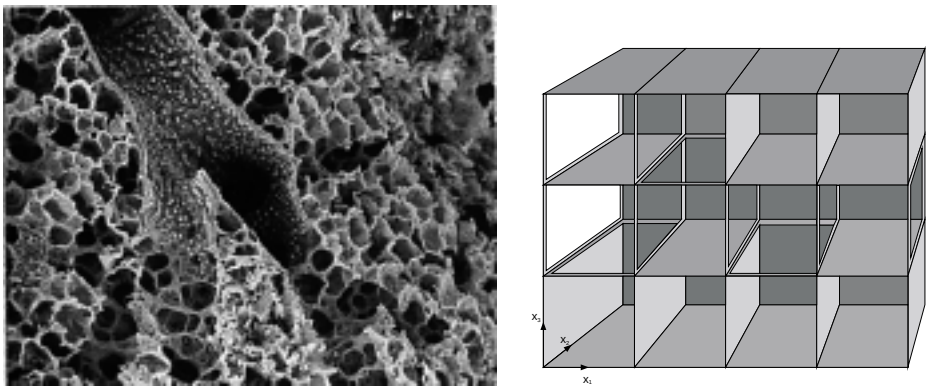

(a) (b)

FIG. 1.1. (a) *Section of lung showing a small bronchiole and many alveoli. Small "pores of Kohn" connecting alveoli are visible (image courtesy of Lawrence Berkeley National Laboratory LungLab Tour, http://imglib.lbl.gov/ImgLib/COLLECTIONS/lung_tour.html).* (b) *Mathematical caricature of alveolar lung tissue.*

time constants. The result is a "sloshing" motion of air between the two neighboring units during a ventilation cycle (*pendelluft*).

Many current models for ventilation by HFO are based on refinements of the work of Otis et al. [22], where the lung is caricatured by an analogous electrical circuit with specified resistance, inductance and capacitance components to describe its global behavior [17]. More detailed differential equation models based on transmission line theory have been derived from the properties of viscous fluid flow in elastic airways [11, 12]. These have been used to study pressure distributions in symmetric and asymmetric branching lung structures [18]. Numerical models for the transport of suspended particles or aerosols in the lung use two or three dimensional fluid flow (governed by the Navier–Stokes equations) for movement of the air through an open-ended rigid structure representing the interior of the lung [6]. Other lung models include alveolar mechanical properties but contain no fluid flow component [8]. However, no models exist that couple detailed gas-flow modeling with the biomechanical properties of the lung at the alveolar level to fully describe pressures and flows during ventilation.

In principle, the mathematical description of air flow through lung tissue is complete in the sense that we can write down equations governing the fluid dynamics of the air, the mechanics of the airway walls, and the coupling between these motions. However, the geometric complexity of the lung precludes numerical solution of these equations for anything but a tiny fraction of the whole lung, such as a few airways or alveoli—Figure 1.1(a) illustrates this complexity, even in a very small section of the lung. In this paper, we describe the application of homogenization theory to derive equations for air velocities, pressures, and solid displacements, averaged over the basic repeating microscopic unit of respiratory lung tissue, namely an alveolus. We make the simplifying assumption that lung tissue at the alveolar level is comprised of an array of units of similar size and shape, as illustrated in a highly idealized form in Figure 1.1(b). This allows us to move from a microscopic to a macroscopic space scale, for example from a single alveolus to an acinus (a respiratory unit consisting of thousands of alveoli), where the equations for macroscopic behavior are determined by

the microscopic geometry. In section 2 we introduce the governing equations in three dimensions, estimate parameters, and nondimensionalize. We then briefly describe the homogenization technique, and the derivation of macroscopic three dimensional equations (section 3, with full details in Appendix A). Even though we eventually consider a simplification to lower spatial dimensions, it is essential to consider the full three dimensional structure in order to describe the interconnected lung wall and fluid. In section 4 we consider the case where lung tissue is assumed to be isotropic, which enables the deduction of macroscopic solid viscosity parameters from measurements of lung bulk elasticity and Poisson ratio.

In section 5 we describe some solutions in one dimension and provide a further simplification of the system to a single augmented diffusion equation for the pressure. Experimental techniques have recently been developed to investigate the response of alveolar tissue to high-frequency pressure oscillations. A device know as an "alveolar capsule" is attached to the pleural surface of the lung, connecting with the alveolar space via a hole which is made in the pleural surface [7]. The capsule contains two transducers, one to generate the input, and the other to record the response of the tissue, as measured by the pressure in the capsule. Parameters measuring the properties of the underlying lung tissue were estimated from the data by fitting to a simple ordinary differential equation model. Such models do not take account of spatial effects, so it is of interest to see how the derived macroscopic spatial system behaves in this type of situation. Thus we consider solutions in one dimension for boundary conditions corresponding to forced ventilation and to this alveolar capsule technique. We conclude with a discussion and some ideas for further research (section 6).

2. Governing equations. Because HFO uses small tidal volumes at relatively high frequencies, we are interested in small perturbations of the relevant variables from some rest state determined by the mean airway pressure (MAP). This pressure maintains the lung at a mean volume, and small oscillations in pressure about the MAP will give small strains in the solid in relation to this rest state. Fluid velocities will be small perturbations about zero, since at the rest state there will be no air flow. Thus we consider linearized Navier–Stokes equations for the flow of air, and linear viscoelasticity of the solid tissue. This framework also means that all pressures are measured relative to MAP.

The governing equations for the fluid-solid system are

$$\rho_f \frac{\partial \mathbf{v}}{\partial t} = \nabla \cdot \underline{\underline{\sigma}} = -\nabla p + \mu \Delta \mathbf{v} \text{ in } D_f, \tag{2.1}$$

$$\nabla \cdot \mathbf{v} = 0 \qquad \text{in } D_f, \tag{2.2}$$

$$\mathbf{v} = \frac{\partial \mathbf{u}}{\partial t} \qquad \text{on } \partial D_f = \partial D_s, \tag{2.3}$$

$$\mathbf{n} \cdot \underline{\underline{\sigma}} = \mathbf{n} \cdot \underline{\underline{\mathcal{T}}} \qquad \text{on } \partial D_f = \partial D_s, \tag{2.4}$$

$$\rho_s \frac{\partial^2 \mathbf{u}}{\partial t^2} = \nabla \cdot \underline{\underline{\mathcal{T}}} \qquad \text{in } D_s, \tag{2.5}$$

where $\mathbf{v}(\mathbf{x}, t)$ is the fluid velocity, $p(\mathbf{x}, t)$ is pressure, and $\mathbf{u}(\mathbf{x}, t)$ is the displacement of the solid from its rest state at MAP. We will always use boldface to denote vectors, and $j \geq 2$ underbars indicate a j-tensor—for simplicity and clarity we also use index notation for some tensor calculations. Thus $\underline{\underline{\sigma}}$ is a 2-tensor describing viscous and

pressure stresses [4] in the fluid:

$$\underline{\underline{\sigma}} = \overbrace{\mu(\nabla \mathbf{v} + (\nabla \mathbf{v})^T)}^{\text{Viscous Stress}} - \overbrace{p\underline{\underline{I}}}^{\text{Pressure Stress}}, \tag{2.6}$$

and $\underline{\underline{\mathcal{T}}}$ is the solid stress tensor describing elastic and viscous stresses [21]:

$$\underline{\underline{\mathcal{T}}} = \overbrace{\frac{2E}{3}\underline{\underline{e}}}^{\text{Elastic Stress}} + \overbrace{\mu_1 \underline{\underline{e}}_t}^{\text{Viscous Stress}}. \tag{2.7}$$

Here $\underline{\underline{e}}$ is the strain tensor given by

$$\underline{\underline{e}} = \frac{\nabla \mathbf{u} + (\nabla \mathbf{u})^T}{2}, \tag{2.8}$$

μ is the fluid viscosity, ρ_f is the fluid density, E is the Young's modulus for the solid, μ_1 is the shear viscosity for the solid, and ρ_s is the solid density. Note that we are assuming the solid is incompressible, which is reasonable since it is essentially composed of collagen and elastin fibers, and water. Also note that because we are assuming small perturbations about a rest state maintained by a mean airway pressure, the Young's modulus and shear viscosity for the solid should correspond to measurements made about the corresponding stretched rest state. This is sometimes referred to as the incremental Young's modulus.

2.1. Parameter estimation. Certain parameters are easy to estimate with confidence. For example, the fluid viscosity and density—those of air—can be found in a variety of texts and data books. We expect the density of the alveolar wall tissue to be approximately that of water. Thus we use

$$\begin{aligned} \mu &= 2 \times 10^{-5} \text{Kg m}^{-1}\text{s}^{-1}, \\ \rho_f &= 1 \text{Kg m}^{-3}, \\ \rho_s &= 10^3 \text{Kg m}^{-3}. \end{aligned} \tag{2.9}$$

It remains to estimate the viscoelastic parameters of the solid. In the simplest case of a static force, we should have

$$\frac{\text{force}}{\text{area}} = \frac{2E}{3}\text{strain}. \tag{2.10}$$

Fukaya et al. [14] carried out a number of experiments on the mechanical properties of the alveolar wall. Using their figures, we can estimate the force, area, and strain and hence get an estimate for E, the Young's modulus. Fukaya et al. [14] measure the force in mg, and 1mg of force is $1 \times 10^{-6}\text{Kg} \times 9.81\text{m s}^{-2} \approx 10^{-5}\text{Kg m s}^{-2}$. Forces in mg and strains are estimated visually from the force-strain curves in Figure 2 of Fukaya et al. [14]. Thus rearranging the above word equation gives

$$E = \frac{\text{force in mg} \times 10^{-5}}{\text{area in m}^2 \times \text{strain}} \times \frac{3}{2}. \tag{2.11}$$

The estimate for cross-sectional area is particularly weak, since Fukaya et al. do not give precise values: "With the aid of a microscope, a smaller piece of tissue

($< 30 \times 30 \times 200\mu$) was separated." This leads us to take an estimate for the area to be $30 \times 30 \times 10^{-12}\mathrm{m}^2 = 9 \times 10^{-10}\mathrm{m}^2$. For example, a force of 2mg gives a strain of 0.58, so we have

$$E = \frac{2 \times 10^{-5}}{9 \times 10^{-10} \times 0.58} \times \frac{3}{2} \approx 5 \times 10^4 \mathrm{Kg\,m^{-1}s^{-2}}. \tag{2.12}$$

Similarly, a force of 3mg for a strain of 0.75 gives $E \approx 6 \times 10^4 \mathrm{Kg\,m^{-1}s^{-2}}$; 5mg for a strain of 0.85 gives $E \approx 10 \times 10^4 \mathrm{Kg\,m^{-1}s^{-2}}$; and 8mg for a strain of 0.95 gives $E \approx 14 \times 10^4 \mathrm{Kg\,m^{-1}s^{-2}}$. As a representative order of magnitude estimate we therefore use $E = 10^5 \mathrm{Kg\,m^{-1}s^{-2}}$.

For the viscous part of solid force generation, we suppose that inertial terms are negligible, and that

$$\frac{\text{dynamic force} - \text{static force}}{\text{area}} = \mu_1 \times \text{rate of change of strain}. \tag{2.13}$$

In the experiments, the tissue is stretched to 90% strain in time T seconds. We use the previous estimate for the cross-sectional area, and estimate the difference between dynamic and static forces, ΔFmg, visually from Figure 4 of Fukaya et al. [14]. Thus we have

$$\mu_1 = \frac{\Delta F \times 10^{-5} \times T}{9 \times 10^{-10} \times 0.9} \mathrm{Kg\,m^{-1}s^{-1}}. \tag{2.14}$$

The measurements $\Delta F = 1.5, T = 30$; $\Delta F = 1.9, T = 14$; and $\Delta F = 3.4, T = 0.5$ give us $\mu_1 \approx 5 \times 10^5 \mathrm{Kg\,m^{-1}s^{-1}}$; $\mu_1 \approx 3 \times 10^5 \mathrm{Kg\,m^{-1}s^{-1}}$; and $\mu_1 \approx 2 \times 10^4 \mathrm{Kg\,m^{-1}s^{-1}}$, respectively. We take $\mu_1 = 10^5 \mathrm{Kg\,m^{-1}s^{-1}}$ as a representative estimate of an appropriate order of magnitude.

The structural damping hypothesis states that the viscosity of the tissue comprising the lung wall is inversely proportional to the frequency of oscillation [13]. This alternative approach is based on the idea that it is the same biomechanical elements which are responsible for both the elastic and viscous stresses in the tissue. We would like to deal in this paper with both standard viscoelasticity and the concept of structural damping, so we introduce an alternative parameter, μ_{SD}, where the subscript SD denotes "structural damping." This parameter describes the contribution of viscous stress, where $\mu_1 = \mu_{SD}/\omega$. With the data described above, we approximate ω by $1/2T$, where T is the duration of stretching in the experiments of Fukaya et al. [14]—thus we are treating the experiments as one half of a complete cycle of stretching and relaxation. These give approximations for μ_{SD} of $8333, 10714$, and 20000—the first two are in particularly good agreement. For simplicity we use these calculations only as a guideline, and take $\mu_{SD} = 10^4 \mathrm{Kg\,m^{-1}s^{-2}}$. We will see in the next section that nondimensionalizing yields identical governing equations for both cases, with the different approaches manifesting themselves in the parameter values.

A summary of all our parameter estimates is given in Table 2.1. We remind the reader that these are based upon measurements taken from Figures 2 and 4 of Fukaya et al. [14], and incomplete knowledge of the cross-sectional area of tissue under investigation. We have also made a number of other assumptions and approximations, and these values only serve as guidelines as to the appropriate order of magnitude.

2.2. Nondimensionalization. We wish to appropriately nondimensionalize the system of governing equations (2.1)–(2.5). We will rescale space by L, the macroscopic

TABLE 2.1
Parameter estimates for the fluid-solid model (2.1)–(2.5).

Parameter	Description	Estimate
μ	Air viscosity	$2 \times 10^{-5}\text{Kg m}^{-1}\text{s}^{-1}$
ρ_f	Air density	1Kg m^{-3}
E	Young's modulus of the alveolar wall	$10^5\text{Kg m}^{-1}\text{s}^{-2}$
μ_1	Shear viscosity of the alveolar wall	$10^5\text{Kg m}^{-1}\text{s}^{-1}$
μ_{SD}	Structural damping viscosity	$10^4\text{Kg m}^{-1}\text{s}^{-2}$
ρ_s	Density of the alveolar wall	10^3Kg m^{-3}

length scale of interest, and time by ω, the frequency of oscillation. Thus dimensionless positions, velocities, and displacements follow naturally—we scale the pressure using ρ_s, the density of the lung wall. Finally, l is the microscopic length scale, the length of a unit cell (alveolar sac in the case of the lung).

$$t^* = \omega t, \quad \mathbf{x}^* = \frac{\mathbf{x}}{L}, \quad \mathbf{v}^* = \frac{\mathbf{v}}{\omega L}, \quad \mathbf{u}^* = \frac{\mathbf{u}}{L}, \quad p^* = \frac{p}{\rho_s \omega^2 L^2}, \tag{2.15}$$

$$\varepsilon = \frac{l}{L}, \quad \rho^* = \frac{\rho_f}{\rho_s}, \quad \mu^* = \frac{\mu}{\rho_s \omega l^2}. \tag{2.16}$$

These rescalings give

$$\rho^* \frac{\partial \mathbf{v}^*}{\partial t^*} = \nabla^* \cdot \underline{\underline{\sigma^*}} = -\nabla^* p^* + \varepsilon^2 \mu^* \Delta^* \mathbf{v}^* \quad \text{in} \quad D_f^*, \tag{2.17}$$

$$\nabla^* \cdot \mathbf{v}^* = 0 \qquad \text{in} \quad D_f^*, \tag{2.18}$$

$$\mathbf{v}^* = \frac{\partial \mathbf{u}^*}{\partial t^*} \qquad \text{on} \quad \partial D_f^* = \partial D_s^*, \tag{2.19}$$

$$\mathbf{n}^* \cdot \underline{\underline{\sigma^*}} = \mathbf{n}^* \cdot \underline{\underline{\mathcal{T}^*}} \qquad \text{on} \quad \partial D_f^* = \partial D_s^*, \tag{2.20}$$

$$\frac{\partial^2 \mathbf{u}^*}{\partial t^{*2}} = \nabla^* \cdot \underline{\underline{\mathcal{T}^*}} \qquad \text{in} \quad D_s^*. \tag{2.21}$$

The dimensionless fluid stress tensor is

$$\underline{\underline{\sigma^*}} = \frac{\underline{\underline{\sigma}}}{\rho_s \omega^2 L^2} = \varepsilon^2 \mu^* (\nabla^* \mathbf{v}^* + (\nabla^* \mathbf{v}^*)^T) - p^* \underline{\underline{I}}, \tag{2.22}$$

and the dimensionless solid stress tensor is given by

$$\underline{\underline{\mathcal{T}^*}} = \frac{\underline{\underline{\mathcal{T}}}}{\rho_s \omega^2 L^2} = \frac{2E^*}{3} \underline{\underline{e^*}} + \mu_1^* \underline{\underline{e^*}}_t. \tag{2.23}$$

Here $\underline{\underline{e}}$ is the strain tensor, given by $\underline{\underline{e^*}} = \underline{\underline{e}}$ (since it is already dimensionless) and

$$E^* = \frac{E}{\rho_s \omega^2 L^2}. \tag{2.24}$$

μ_1^* depends on the choice of the standard viscous term, or of that which takes account of the structural damping coefficient:

$$\mu_1^* = \frac{\mu_1}{\rho_s \omega L^2} \quad \text{or} \quad \mu_1^* = \frac{\mu_{SD}}{\rho_s \omega^2 L^2}. \tag{2.25}$$

Thus the form of the dimensionless system is identical for both cases, with differences only arising once particular parameters are chosen.

A typical alveolar sac has a length, l, of approximately $200\mu\text{m} = 2 \times 10^{-4}\text{m}$, and the large length scale—for example, the length of an acinus—is about $L = 1\text{cm} = 10^{-2}\text{m}$. Using the parameter values estimated in the previous section, we have

$$\rho^* = 10^{-3}, \quad \mu^* = \frac{1}{2\omega}, \quad E^* = \frac{10^6}{\omega^2}, \tag{2.26}$$

and

$$\begin{aligned} &\text{standard viscoelasticity: } \mu_1^* = \frac{10^6}{\omega}, \\ &\text{structural damping: } \mu_1^* = \frac{10^5}{\omega^2}. \end{aligned} \tag{2.27}$$

3. Homogenization. In this section we give an outline of the procedure for deriving equations for macroscopic behavior—we refer the reader to Appendix A for the details. It would be feasible to solve (2.17)–(2.21) on a realistic lung geometry for only a small number of alveoli, certainly not for the thousands which make up even a single acinus. Our approach is to treat the structure as an array of repeating cells (see Figure 3.1), representing alveoli, and to consider the average flow and deformation in a cell neglecting the microscopic details. We consider the full three dimensional structure of the lung tissue because the interconnectivity of the lung wall and fluid cannot be adequately described by a lower dimensional caricature—see Figure 3.1.

Mathematically we consider the system variables as functions of independent variables $\mathbf{x}$ and $\mathbf{y}$, where $\mathbf{y} = \varepsilon^{-1}\mathbf{x}$. Here the crucial assumption is that variations on the small scale (i.e., with $\mathbf{y}$) are independent from those on the large scale $\mathbf{x}$, and thus we treat $\mathbf{x}$ and $\mathbf{y}$ as independent variables so that

$$\nabla f(\mathbf{x}, \mathbf{y}) = \nabla f(\mathbf{x}, \varepsilon^{-1}\mathbf{x}) = \nabla_{\mathbf{x}} f + \varepsilon^{-1}\nabla_{\mathbf{y}} f. \tag{3.1}$$

When considering ventilation of the lung we look for time-harmonic solutions (i.e., solutions proportional to $\exp(i\omega t) = \exp(it^*)$—henceforth we drop the asterisks for notational simplicity). We then seek solutions which are asymptotic power series in ε. For example, the form for the fluid velocity would be

$$\mathbf{v}(\mathbf{x}, \mathbf{y}, \varepsilon) = \mathbf{v}^0(\mathbf{x}, \mathbf{y}) + \varepsilon \mathbf{v}^1(\mathbf{x}, \mathbf{y}) + \varepsilon^2 \mathbf{v}^2(\mathbf{x}, \mathbf{y}) + \mathcal{O}(\epsilon^3). \tag{3.2}$$

Similar expansions for the pressure p and the material displacement $\mathbf{u}$ and substitution of these series yields a system of linear equations for each successive order of ε.

Analysis of various subsystems and averaging over the unit cell lead to the following equations for the mean quantities $\mathbf{V}, P, \mathbf{U}$:

$$\begin{aligned} \mathbf{V} - i\phi\mathbf{U} &= -\underline{\underline{K}}\,(\nabla P - \rho\mathbf{U}), \\ \nabla \cdot (\mathbf{V} - i\phi\mathbf{U}) &= i\left(\underline{\underline{\alpha}} : \frac{\nabla\mathbf{U} + (\nabla\mathbf{U})^T}{2} + \beta P\right), \\ i\rho\mathbf{V} - \mathbf{U} &= \nabla \cdot \left(\underline{\underline{\underline{\underline{C}}}}\frac{\nabla\mathbf{U} + (\nabla\mathbf{U})^T}{2} + \underline{\underline{\alpha}} P\right), \end{aligned} \tag{3.3}$$

where $A : B$ indicates the matrix inner product of A and B (i.e., the sum of elementwise products); ϕ is the fluid volume fraction, often called porosity; and the

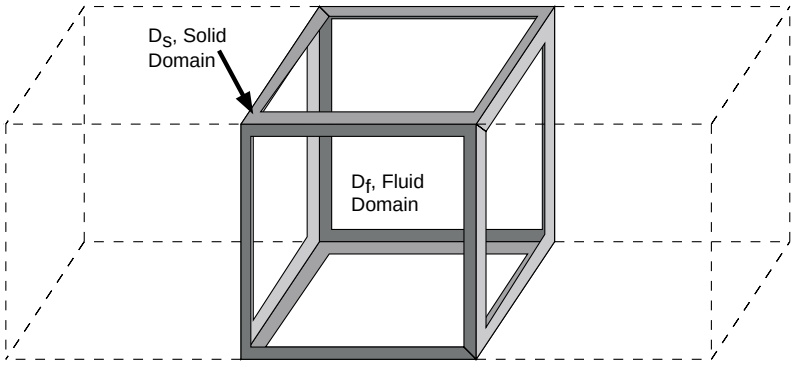

FIG. 3.1. *Basic repeating unit.*

parameters $\underline{\underline{K}}$, $\underline{\underline{\alpha}}$, β, and $\underline{\underline{\underline{C}}}$ are determined by the geometry of the unit cell. The complete derivation of these results is given in Appendix A.

Thus all the parameters in the macroscopic system (3.3) are defined in terms of the microstructure. Note that the three equations in (3.3) correspond to flow driven by pressure gradients, conservation of mass, and conservation of momentum, in that order. We interpret $(V - i\phi U)$ as fluid velocity relative to the motion of the solid. The equations indicate that, macroscopically, lung tissue is compressible—for example, changes in air pressure will allow the tissue as a whole to dilate, even though the walls themselves cannot.

When $\omega = 0$, that is, in the situation where there are no temporal oscillations, the system (3.3) reduces to Darcy's law for flow through porous media ($\mathbf{V} = -\underline{\underline{K}}\nabla P$, and $\nabla \cdot \mathbf{V} = 0$) where $\underline{\underline{K}}$ is called the permeability tensor. Here $\underline{\underline{K}}$ depends only on the geometry of the porous media, and the fluid density and viscosity. If the structure is isotropic, then permeability is given by a scalar quantity, K. Permeability is related to the reciprocal of the resistance to flow, for example the resistance to the flow of air through respiratory tissue, as estimated by Davey and Bates [7]. The difference is that lung resistance, R, is measured as a property of the whole of the tissue region of interest. R increases linearly with the length, L_R, of this tissue region, and scales according to the reciprocal of the cross-sectional area, A_R. This means that the relationship between R and K should be $K = L_R/(RA_R)$—this is very crude, and does not take account of the shape or structural variations within the region, etc. Nevertheless, we use it to make an estimate for K which we will use as a starting point for the calculation of solutions—a representative estimate of resistance from Davey and Bates [7] is $R = 1.0\text{KPa}\,\text{sml}^{-1} = 10^7\text{Kgm}^{-4}\text{s}^{-1}$, and we estimate $L_R = 10^{-2}\text{m}$ and $A_R = 10^{-4}\text{m}^{-4}$, which gives a very rough estimate of the permeability as $K \approx 10^{-7}\text{m}^3\text{sKg}^{-1}$. The corresponding dimensionless value is $K^* \approx 10^{-4}/\omega$—see (3.5) for the appropriate rescaling.

If there were no viscous component to the stress in the solid ($\mu_1 = 0$), then (3.3) reduces to Biot's equations for oscillatory flow through a purely elastic solid, which were first derived empirically [1]. More recently, homogenization theory has also been used to arrive at the same equations [2, 20].

With no fluid flow, and just a constant, homogeneous inflating pressure (e.g., lungs maintained at constant volume by MAP), we get a macroscopic stress–strain relation for the solid at that pressure. The parameters of this stress strain relationship, the

fourth rank viscoelasticity tensor C_{ijkl}, can be related to experimental measurements, particularly if we assume isotropic behavior—see section 4.

It is also instructive to include the dimensional macroscopic equations and corresponding parameters. In particular, the dependence on frequency is clear:

$$\begin{aligned} \mathbf{V} - i\omega\phi\mathbf{U} &= -\underline{\underline{K}}\left(\nabla P - \omega^2\rho_f\mathbf{U}\right), \\ \nabla\cdot(\mathbf{V} - i\omega\phi\mathbf{U}) &= i\omega\left(\underline{\underline{\alpha}} : \tfrac{\nabla\mathbf{U}+(\nabla\mathbf{U})^T}{2} + \beta P\right), \\ i\omega\rho_f\mathbf{V} - \rho_s\omega^2\mathbf{U} &= \nabla\cdot\left(\underline{\underline{\underline{\underline{C}}}}\tfrac{\nabla\mathbf{U}+(\nabla\mathbf{U})^T}{2} + \underline{\underline{\alpha}}P\right), \end{aligned} \tag{3.4}$$

where the parameter rescalings are

$$\underline{\underline{K}} = \frac{\underline{\underline{K^*}}}{\rho_s\omega}, \quad \underline{\underline{\alpha}} = \underline{\underline{\alpha^*}}, \quad \beta = \frac{\beta^*}{\rho_s\omega^2L^2}, \quad \underline{\underline{\underline{\underline{C}}}} = \rho_s\omega^2L^2\underline{\underline{\underline{\underline{C^*}}}}. \tag{3.5}$$

4. Assumption of macroscopic isotropy. If we assume that the macroscopic behavior of lung tissue is isotropic, then the solid stress must take the form

$$\underline{\underline{\underline{\underline{C}}}}\,\underline{\underline{e}} = \frac{\hat{E}}{1+\hat{\nu}}\left(\underline{\underline{e}} + \frac{\hat{\nu}}{1-2\hat{\nu}}\,\theta\underline{\underline{I}}\right) + i\hat{\mu}_1\,\underline{\underline{e}} + i\hat{\mu}_2\,\theta\underline{\underline{I}}, \tag{4.1}$$

where $\underline{\underline{e}}$ and $\theta = \mathrm{Trace}\,(\underline{\underline{e}})$ are the macroscopic strain tensor and dilation, respectively. This assumption allows us to use experimental data to estimate all these scalars. The Young's modulus, $\hat{E}$, and Poisson ratio, $\hat{\nu}$, for bulk lung tissue have been experimentally measured and theoretically predicted. The form of the equations means that $\hat{\mu}_1$ and $\hat{\mu}_2$ are then determined by the macroscopic properties $\hat{E}$ and $\hat{\nu}$ and by the microscopic elastic and viscous properties of the lung wall.

In particular, we show in Appendix B how, given $E, \mu_1, \hat{E}$, and $\hat{\nu}$, it follows that

$$\hat{\mu}_1 = \mu_1\frac{3\hat{E}}{2E(1+\hat{\nu})}, \quad \hat{\mu}_2 = \mu_1\frac{3\hat{E}\hat{\nu}}{2E(1+\hat{\nu})(1-2\hat{\nu})} \tag{4.2}$$

and

$$\alpha = \frac{3\hat{E}}{2E(1-2\hat{\nu})} - 1, \quad \beta = 3\left(\frac{3\hat{E}}{2E(1-2\hat{\nu})} + \phi - 1\right)\left(\frac{2E}{3} + i\mu_1\right)^{-1}, \tag{4.3}$$

so that given an estimate for K, the whole system is specified.

At typical mean airway pressure ($\approx 20\mathrm{cmH_2O} \approx 2000\mathrm{Kg\,m^{-1}s^{-2}}$) for HFO, the Young's modulus of lung tissue has been estimated to be about 4 times this pressure [15, 16] ($\approx 8000\mathrm{Kg\,m^{-1}s^{-2}}$), giving a dimensionless value of $\hat{E} \approx \frac{8\times10^4}{\omega^2}$. The Poisson ratio for bulk lung tissue at this mean airway pressure has been estimated to be $\hat{\nu} \approx 0.3$ [16].

Recall that the dimensionless parameters governing viscoelasticity of the solid are $E \approx 10^6/\omega^2$ and $\mu_1 \approx 10^6/\omega$ (standard viscoelasticity) or $\mu_1 \approx 10^5/\omega^2$ (structural damping). Using the above values for $\hat{E}$ and $\hat{\nu}$, we have for standard viscoelasticity

$$\hat{\mu}_1 \approx \frac{10^5}{\omega}, \quad \hat{\mu}_2 \approx \frac{0.75\times10^5}{\omega}, \quad \alpha \approx -0.7, \quad \beta \approx \frac{3\times10^{-6}\omega^2}{2+3i\omega} \tag{4.4}$$

and for structural damping

$$\hat{\mu}_1 \approx \frac{10^4}{\omega^2}, \quad \hat{\mu}_2 \approx \frac{0.75\times10^4}{\omega^2}, \quad \alpha \approx -0.7, \quad \beta \approx \frac{3\times10^{-5}\omega^2}{20+3i}. \tag{4.5}$$

We have rounded all these values appropriately, since using more precision would falsely imply that these estimates are very accurate. To conclude this section as we began, we rewrite the solid stress with our parameter estimates, for standard viscoelasticity, as

$$\underline{\underline{\underline{\underline{C}}}}\,\underline{\underline{e}} = \frac{10^4}{\omega^2}(6+10\omega i)\left(\underline{\underline{e}} + 0.75\,\theta\underline{\underline{I}}\right), \tag{4.6}$$

and for structural damping as

$$\underline{\underline{\underline{\underline{C}}}}\,\underline{\underline{e}} = \frac{10^4}{\omega^2}(6+i)\left(\underline{\underline{e}} + 0.75\,\theta\underline{\underline{I}}\right), \tag{4.7}$$

where we have again rounded the values for clarity, e.g., $\hat{E}/(1+\hat{\nu}) = 6.1538\times 10^4/\omega^2 \approx 6\times 10^4/\omega^2$. Note that we have clearly indicated how these values change with the ventilation frequency, ω.

5. Solutions to the macroscopic equations in one dimension. To develop our understanding of macroscopic lung tissue behavior it is useful to study solutions of the one dimensional equations, where primes indicate spatial derivatives:

$$V - i\phi U = -K(P' - \rho U), \tag{5.1}$$

$$V' - i\phi U' = i(\alpha U' + \beta P), \tag{5.2}$$

$$i\rho V - U = \left(CU'' + \alpha P'\right). \tag{5.3}$$

Here we have simply assumed that $\mathbf{V} = V(x)\mathbf{e}_x$, where $\mathbf{e}_x$ denotes the unit vector in the x-direction, and similarly for the other variables, so that all variation is purely in the x-direction.

In order to solve this eighth order system of complex ODEs, we separate into real and imaginary parts. In Appendix C we show how this leads to a system of eight ODEs, for which explicit solutions can be found. We consider two types of boundary conditions, one corresponding to forced ventilation and one to the application of the alveolar capsule technique, where small pressure oscillations are applied at the pleural surface to study flow in the alveolar region [7].

5.1. Solutions with forced ventilation boundary conditions. Forced ventilation has a specified sinusoidally varying input pressure, P_a, with arbitrary phase, and zero displacement of the solid at the opening, $x = 0$. At the pleural surface, $x = \mathcal{L}$, the pressure is a constant, equal to the mean airway pressure. We also require that the fluid velocity is equal to the velocity of the solid (lung tissue), so that no gas actually flows out through the "end" of the lung:

$$\begin{gathered} P_r(0) = P_a, \quad P_i(0) = 0, \quad U_r(0) = 0, \quad U_i(0) = 0, \\ V_r(\mathcal{L}) = -\phi U_i(\mathcal{L}), \quad V_i(\mathcal{L}) = \phi U_r(\mathcal{L}), \quad P_r(\mathcal{L}) = 0, \quad P_i(\mathcal{L}) = 0. \end{gathered} \tag{5.4}$$

Note that while we have developed the macroscopic equations in dimensionless form, we illustrate solutions in dimensional variables, which we feel are of real interest physiologically. This is because the nondimensionalization used includes a rescaling of time which depends on frequency, a parameter which we actually would like to vary, in order to establish how the response of lung tissue may depend on the forcing

frequency. Dimensional solutions are calculated simply by applying the rescalings in equation (2.15) to dimensionless values.

In section 2.1 we introduced the structural damping hypothesis as an alternative model for viscoelasticity. We wish to explore the behavior of the system representing lung tissue for both possibilities. We remind the reader that in the dimensionless system this simply corresponds to a change in the parameters that depend on μ_1^*. Here we concentrate on the standard case, and then we discuss the differences seen when applying the alternative model. For all solutions we illustrate the magnitude and phase of oscillation.

An example of the solution for forced ventilation boundary conditions (5.4) is shown in Figure 5.1(a). The magnitude of pressure fluctuations decreases monotonically from the airway opening ($x = 0$), but velocities and displacements increase; penetration into the lung of displacements and strains decrease with increasing frequency, although the velocity and pressure remain the same. The displacement and strain are approximately $\pi/2$ radians out of phase with the fluid velocity and pressure oscillations, although there is very little variation in phase with the distance from the opening. This means that motion is always in the same direction at all locations in the lung.

The increase of velocity with distance seems counterintuitive, since the pressure gradient, which drives the flow, is clearly decreasing in magnitude. This can be explained by the fact that at $x = 0$ the displacement is constrained to be zero, but as the displacement increases away from the opening, this implies a motion of the solid, which adds to the velocity of the fluid from a stationary frame of reference. The velocity of air relative to the solid does decrease in line with the pressure gradient, and in fact plots of this (not shown for brevity) confirm that the relative velocity satisfies $V - i\phi U = -KP'$, as expected. Note that for the range of frequencies in these figures ($5-20\text{s}^{-1}$) changes in frequency do not have very much effect on absolute and relative gas velocities.

Calculations for the one dimensional system with structural damping and forced ventilation boundary conditions, given by (5.4), show some interesting differences from the standard case—see Figure 5.1(b). There are significant phase differences which mean that the solutions give motion in opposite directions within the tissue. In addition, the fluid velocity and pressure now have a significant dependence on the frequency of oscillation. We note that on larger domains the phase differences are even larger and magnitudes no longer vary monotonically—however, it is not clear whether larger domain sizes are physiologically relevant.

One common feature with both standard viscoelasticity and the structural damping hypothesis is that they have the same ordering of solutions with frequency. For example, compare the orderings of displacement and strain in Figure 5.1, which both decrease as the frequency increases.

Because our estimate of tissue permeability is quite crude, it is important to consider how changes in permeability are reflected in model solutions. With K a factor of 10 smaller, oscillations propagate less far into the tissue, and strains decay to zero before the pleural surface (solutions not shown for brevity). For permeability a factor of 10 larger, the pressure oscillations propagate further, and strains decay less before the pleural surface, which has important implications with regard to tissue damage. If we consider the same changes with the structural damping hypothesis the situation is similar.

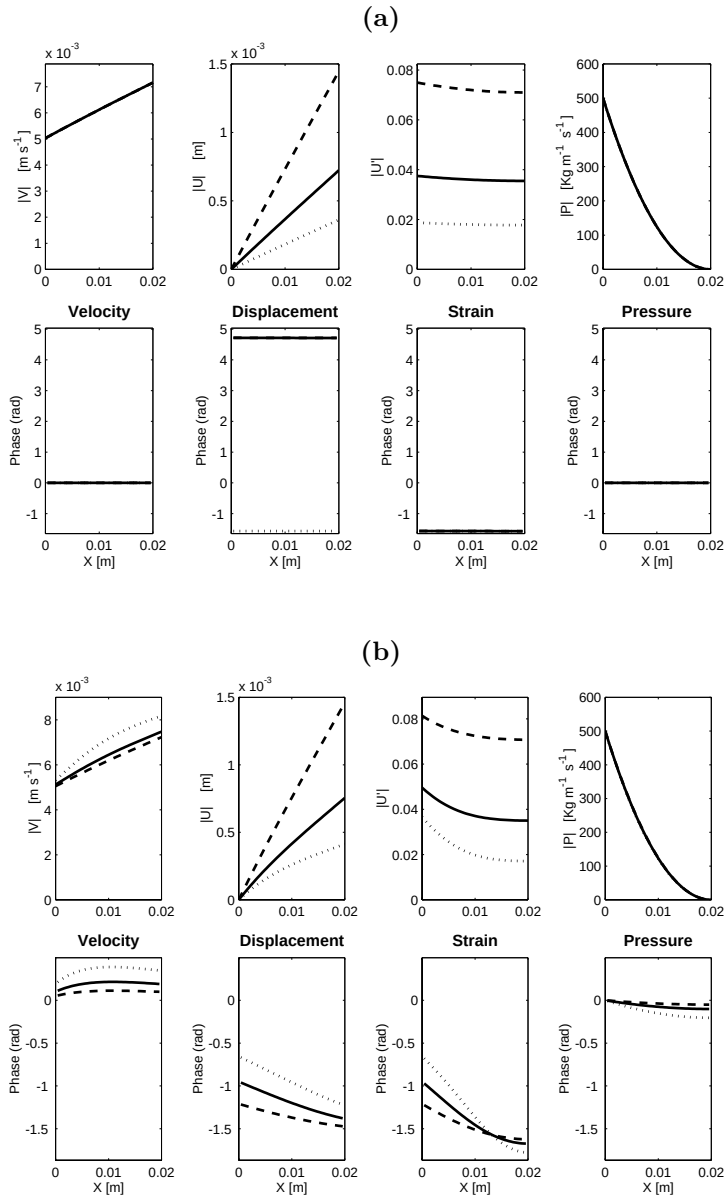

FIG. 5.1. (a) *Solution of the one dimensional system of homogenized equations* (5.1)–(5.3) *for the macroscopic gas velocity, solid displacement, and gas pressure in the lung. The boundary conditions, given by* (5.4)*, correspond to forced ventilation. Frequencies are* 5s^{-1} *(dashed line),* 10s^{-1} *(solid line), and* 20s^{-1} *(dotted line). Dimensional solutions are shown using the rescalings in* (2.15)*. Increasing the frequency does not affect absolute gas velocities, but decreases displacements and strains. Dimensionless parameter values are* $K = 10^{-3}, \mathcal{L} = 10, \beta = (3\times10^{-6}\omega^2)/(2+3i\omega), C = (1.05 + 1.75i\omega) \times 10^5/\omega^2, \phi = 0.99, \rho_f = 10^{-3}, \alpha = -0.7$*, and the dimensionless amplitude of forced pressure oscillations is* $P_a = 5000/\omega^2$*, chosen so that the dimensional amplitude is independent of frequency.* (b) *With viscoelastic terms according to the structural damping hypothesis, forced ventilation boundary conditions* (5.4) *give solutions to* (5.1)–(5.3) *whose magnitudes and phases are more strongly modulated according to frequency and spatial position. In particular, the phase modulation indicates motion in opposite directions at different depths in the lung. Frequencies, line types, and parameters are as in part* (a)*, except for* $\beta = (3\times10^{-5}\omega^2)/(20+3i), C = (1.05+0.175i)\times 10^4/\omega^2$.

We also have considered how solutions for a fixed frequency vary as the solid viscosity changes. Increasing the viscosity has little effect on the solutions for standard viscoelasticity, at least at the parameter values used for the solutions described above. Decreasing the viscosity, however, leads to a stronger spatial dependence of the strain in the tissue, with a greater strain at the airway opening ($x = 0$) but a stronger decay so that the strain at the pleural surface is less than that found before. Interestingly, with the structural damping hypothesis, changing the viscosity seems to have very little effect, at least for the ranges considered.

5.1.1. Solutions with alveolar capsule boundary conditions. Here a capsule is attached to the pleura, connected to the alveolar space by a small hole, and an oscillator in the capsule applies very high frequency pressure oscillations to the underlying region of tissue [7]. Pressure transducers are used to characterize the response of alveolar tissue to frequencies of the order of 200s^{-1} by fitting the data to a simple ordinary differential equation model which incorporates the elasticity of the lung, flow resistance, and fluid inertia. This approach neglects spatial variation and the possibility that a component of flow resistance is due to viscous deformation of the lung tissue, which as we have already discussed, may itself depend on the frequency of oscillation. Thus, we describe solutions at the appropriate frequency range, with and without the structural damping hypothesis, to get some insight into the possible importance of these effects.

We take the capsule to be located at $x = 0$, and $x = \mathcal{L}$ to be the position at which the pressure oscillations are assumed to decay to zero, lung tissue is not displaced, and fluid velocities are zero. This decay will occur over a short distance relative to the length scale of the whole lung, due to the high-frequency, small-amplitude oscillations used in this experimental procedure [7]. The small amplitude means that within a short distance there is a large volume of air in the rest of the lung which is maintained at the mean airway pressure. At $x = 0$ we have the pressure forcing P_a, and note that we must allow displacement of the pleural surface and capsule at this end:

$$P_r(0) = P_a, \quad P_i(0) = 0,$$

$$V_r(\mathcal{L}) = 0, \quad V_i(\mathcal{L}) = 0, \quad U_r(\mathcal{L}) = 0, U_i(\mathcal{L}) = 0, \tag{5.5}$$

$$P_r(\mathcal{L}) = 0, \quad P_i(\mathcal{L}) = 0.$$

Figure 5.2(a) illustrates solutions for the alveolar capsule boundary conditions (5.5), with standard viscoelastcity. We include frequencies of $100, 200$, and 400Hz, appropriate for the higher frequencies used in the alveolar capsule experiments of Davey and Bates [7].

The magnitude of pressure oscillations decreases with distance from the capsule, and the permeability and elastic coefficients will determine how far into the lung tissue significant perturbations persist. For example, decreasing the permeability gives similar behavior, with oscillations in pressure, fluid velocity, and solid displacement decaying to zero in a shorter distance from the source of pressure oscillations on the pleural surface. Changing the frequency, at least in the range illustrated, gives very similar solutions, with apparently identical velocity and pressure magnitudes.

Figure 5.2(b) illustrates that with alveolar capsule boundary conditions, the higher frequencies (100–200Hz) which are appropriate mean that the propagation of oscillations is much reduced but that the phase depends strongly on the distance from the capsule.

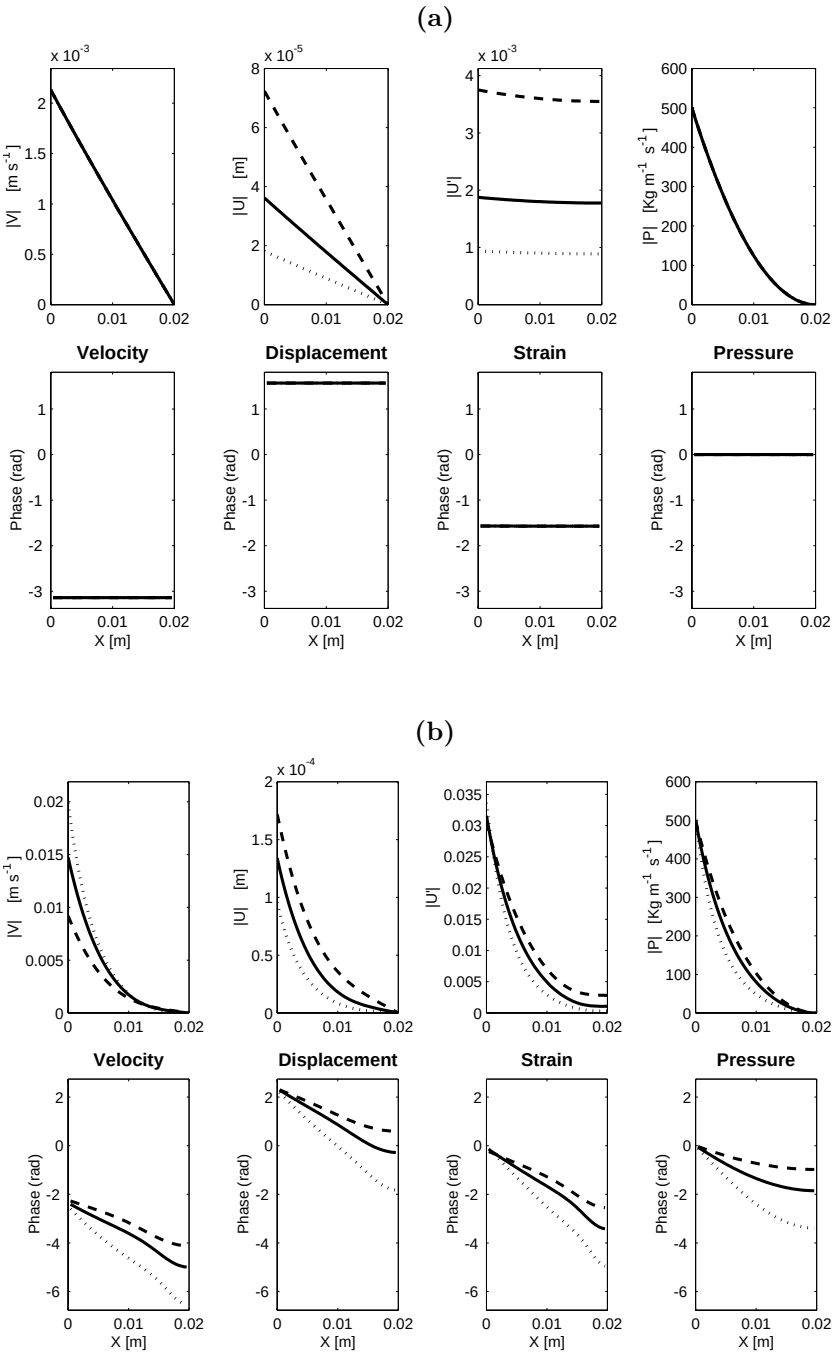

FIG. 5.2. (a) *Solution of the one dimensional system, with the same parameters as in Figure* 5.1*, but with the amended boundary conditions for alveolar capsule oscillation given by* (5.5)*. Frequencies are* 100s^{-1} *(dashed line),* 200 *(solid line), and* 400 *(dotted line), appropriate for the higher frequencies used in the alveolar capsule experiments we have described* [7]. (b) *At the higher frequencies of alveolar capsule oscillation, the structural damping hypothesis makes a significant difference—propagation is markedly reduced, and there are large phase variations. Frequencies are* 100Hz *(solid line),* 200Hz *(dotted line), and* 400Hz *(dashed line). The other parameters are as in Figure* 5.1(b).

5.2. Simplification to pressure diffusion. We have seen that $|\hat{\beta}| \ll 1$ and $\rho \ll 1$, so an interesting simplification is to set $\hat{\beta} = \rho = 0$ in (5.1)–(5.3), which gives, in one dimension,

$$V - i\phi U = -KP', \tag{5.6}$$

$$V' - i\phi U' = i\alpha U', \tag{5.7}$$

$$-U = \left(CU'' + \alpha P'\right). \tag{5.8}$$

Taking the divergence of (5.6) and substituting into (5.7),

$$i\alpha U' = -KP'. \tag{5.9}$$

In the interests of further simplifying the system, we now take the inertial term on the left of (5.8) to be negligible. We will see that this allows us to derive a single equation for the augmented diffusion of the pressure. With the above simplification, (5.8) becomes

$$0 = (\bar{E} + i\bar{\mu})U'' + \alpha P', \tag{5.10}$$

where

$$\bar{E} = \frac{\hat{E}}{1+\hat{\nu}}\left(1 + \frac{\hat{\nu}}{1-2\hat{\nu}}\right); \quad \bar{\mu} = \hat{\mu}_1 + \hat{\mu}_2. \tag{5.11}$$

If we then integrate (5.10) with respect to x,

$$0 = (\bar{E} + i\bar{\mu})U' + \alpha P + P^0, \tag{5.12}$$

and since we have assumed that pressures are measured with reference to some airway opening pressure, and strains are measured with reference to the resting lung volume at that pressure, we have that $P^0 = 0$, and therefore

$$U' = -\frac{\alpha P}{\bar{E} + i\bar{\mu}}. \tag{5.13}$$

Substituting into (5.9) then gives

$$i\alpha U' = -\frac{i\alpha^2 P}{\bar{E} + i\bar{\mu}} = -KP''. \tag{5.14}$$

This then gives us a single diffusion-like equation for the complex pressure P:

$$iP = \frac{(\bar{E} + i\bar{\mu})K}{\alpha^2}P''. \tag{5.15}$$

It is interesting to revert to time derivatives to see more clearly how this system relates to the standard diffusion equation—writing $\tilde{P}(x,t) = e^{it}P(x)$:

$$\tilde{P}_t = \frac{EK}{\alpha^2}\tilde{P}_{xx} + \frac{\mu K}{\alpha^2}\tilde{P}_{xxt}. \tag{5.16}$$

In essence there is straightforward diffusion of the pressure, augmented by an additional viscous term. In the frequency domain this is an easy system to solve. We begin by setting $P = P_r + iP_i$, and substituting into (5.15) gives

$$P_r'' = \left(\frac{\mu}{E}P_r - P_i\right)\frac{\alpha^2 E}{K(E^2+\mu^2)}, \tag{5.17}$$

$$P_i'' = \left(P_r + \frac{\mu}{E}P_i\right)\frac{\alpha^2 E}{K(E^2+\mu^2)}. \tag{5.18}$$

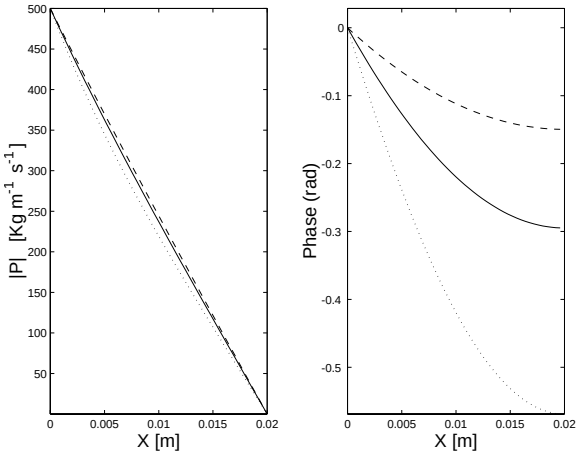

FIG. 5.3. *Solution of the reduced one dimensional system* (5.15) *for pressure in the lung, with boundary conditions, given by* (5.20)*, corresponding to forced ventilation. With the structural damping hypothesis, the reduced model gives slightly decreased penetration with increasing frequency, and strong phase dependence on depth into the lung. Frequencies are* 5s^{-1} *(dashed line),* 10s^{-1} *solid line), and* 20s^{-1} *(dotted line). Parameter values are the same as the relevant values in Figure* 5.1(b).

Setting $Q_r = P_r'$ and $Q_i = P_i'$, we generate a fourth order system,

$$\mathbf{X}' = \begin{pmatrix} 0 & 0 & 1 & 0 \\ 0 & 0 & 0 & 1 \\ \dfrac{\alpha^2\mu}{K(E^2+\mu^2)} & -\dfrac{\alpha^2 E}{K(E^2+\mu^2)} & 0 & 0 \\ \dfrac{\alpha^2 E}{K(E^2+\mu^2)} & \dfrac{\alpha^2\mu}{K(E^2+\mu^2)} & 0 & 0 \end{pmatrix} \mathbf{X}, \tag{5.19}$$

where $\mathbf{X} = (P_r, P_i, P_r', P_i')^T$.

As with the full one dimensional system, we would like to study solutions with standard viscoelasticity and the structural damping hypothesis. However, we do not need two types of boundary conditions, since with this simpler system those for forced ventilation and alveolar capsule oscillations are the same. We consider sinusoidally oscillating input pressure of amplitude P_a at one end ($x = 0$), and at the other end ($x = \mathcal{L}$) the pressure measured with reference to MAP should be zero:

$$P_r(0) = P_a, \quad P_i(0) = 0, \quad P_r(\mathcal{L}) = 0, \quad P_i(\mathcal{L}) = 0. \tag{5.20}$$

Solutions of the reduced model (5.15) with standard viscoelasticity show that pressure oscillations decay with distance from the airway opening, in a similar fashion to the pressure in the full system (omitted for brevity, but see the pressure plots in Figure 5.1(a)); this decay has virtually no dependence on frequency, and there is very little change in phase across the domain.

As with the full one dimensional system, applying the structural damping hypothesis gives somewhat different behavior, as illustrated in Figure 5.3. The penetration of pressure oscillations into the domain is weakly dependent on frequency, and there is a

significant variation in phase. However, these solutions do illustrate the limitations of this reduced model, in that they fail to capture the more complex dynamics indicated for the full system in Figure 5.1(b).

6. Discussion. In this paper we have described how homogenization theory can be used to derive macroscopic equations for average air flows and solid tissue displacements in respiratory lung tissue. This is an important step because the vast number of alveoli in the lung means that it is not feasible to study such flows in a realistic computational model of the lung. Our hope is that such a macroscopic description can be tied to computational and analytical studies of the larger scale flows seen in the conducting airways of the lung.

A study of air flow in the lung is itself very interesting, but perhaps more importantly has many practical applications. One such application is to the ventilation of premature neonates, whose lungs are particularly susceptible to ventilator induced tissue damage. High-frequency ventilation is often used because the smaller breath volumes required reduce the large swings in lung volume seen with conventional techniques. This in turn can reduce the distension of the alveolar walls and hence alleviate stretch-induced damage.

We have shown how the macroscopic properties of respiratory tissue depend on microstructural details, and also how we can use experimental data to estimate the governing parameters. In section 5 we described the calculation of solutions in one dimension using these parameter estimates, and illustrated the significant differences in solution behavior when the alveolar wall is assumed to obey the structural damping hypothesis [13], as opposed to standard linear viscoelasticity. This alternative hypothesis is based upon the idea that it is the same microstructural elements which are responsible for both the elastic and viscous response to deformation. These mechanical interactions operate at a far smaller scale even than that of a single cell of the alveolar wall.

From the form of the homogenized equations, and in accordance with intuition, displacements and strains for the case of standard viscoelasticity are $\pi/2$ out of phase with gas velocities and pressures. Thus velocities are at their maximum when displacements are zero. In contrast, structural damping gives a significant spatial variation of phase, which indicates motion in opposite directions at different locations within the lung tissue. There are some parallels between this and the concept of pendelluft [22], where lung units with different time constants fill and empty out of phase, leading to local flow counter to the direction of ventilation at the trachea. Comparing Figures 5.1(a) and (b), we see that, along with structural damping giving such phase differences, there are small changes in the magnitudes of oscillations. One of the principal motivations behind high-frequency ventilation is that it should help prevent lung tissue damage, and our solutions bear this out, with increasing frequencies leading to decreases in strain. This ordering of magnitudes with frequency is the same for both formulations of viscoelasticity.

Additional investigations show that spatial effects are more prominent on longer domains, and that structural damping then leads to larger strains within the tissue, indicating an increased risk of tissue damage in this regime. Figure 6.1(a) shows the solution over 20cm of lung tissue, with the same parameters as in Figure 5.1(a), and Figure 6.1(b) shows the corresponding case with structural damping. The prediction that structural damping may lead to higher than expected strains may be important from the point of view of patient care, since many existing models used to evaluate ventilation are based on the standard approach and may underestimate the potential

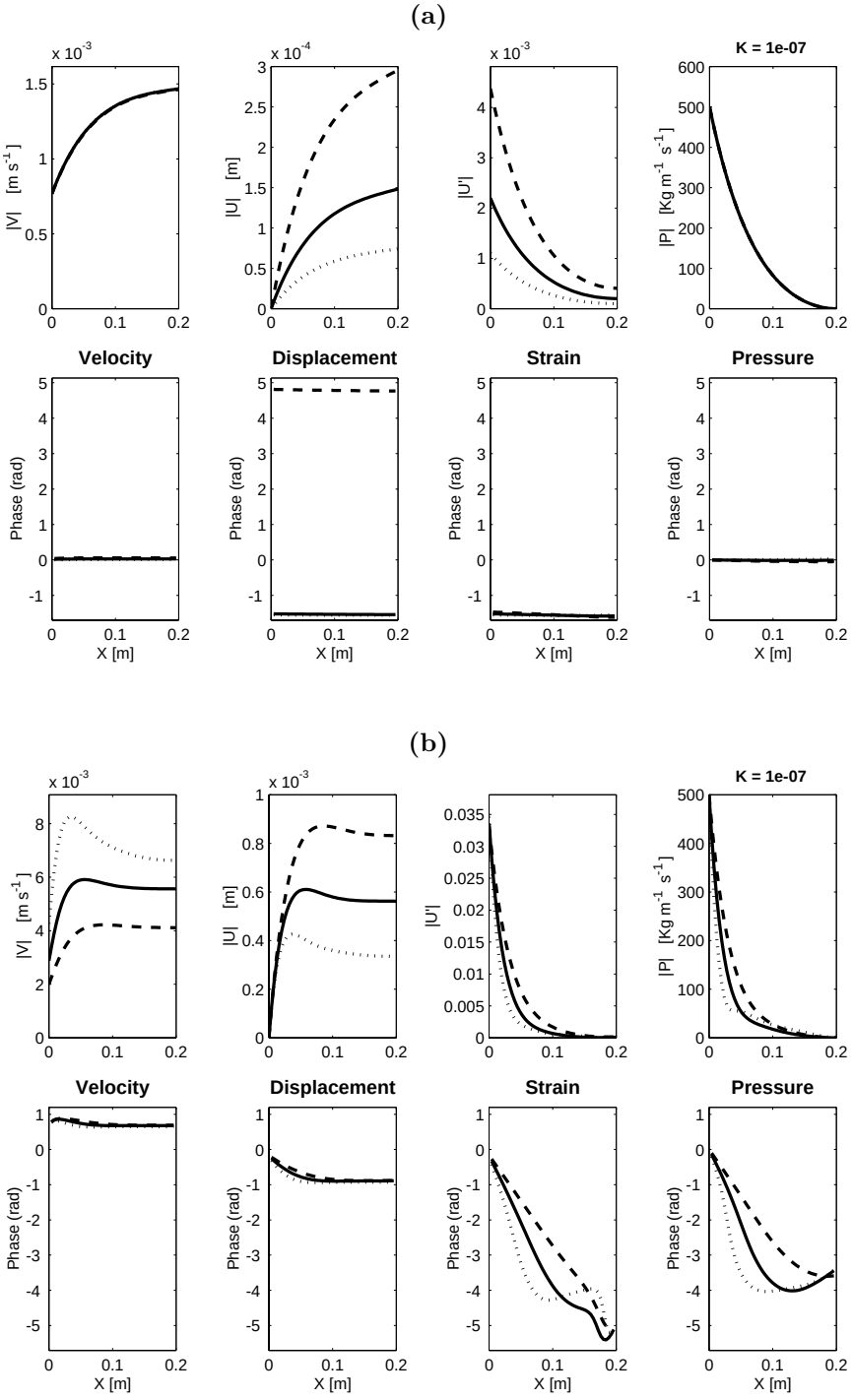

FIG. 6.1. (a) *Over longer domains, spatial effects are more prominent. Solutions are shown for the one dimensional system of homogenized equations* (5.1)–(5.3)*, with forced ventilation boundary conditions* (5.4)*, and standard viscoelasticity. Frequencies, line types, and parameters are as in Figure* 5.1. (b) *With structural damping, solutions are even more strongly modulated in space, with larger tissue strains which indicate an increased likelihood of lung damage. Apart from the increased domain length, all details are as in Figure* 5.1(b).

for adverse effects.

Structural damping has a more pronounced effect at the higher frequencies appropriate for the alveolar capsule method, with all variables subject to phase lags up to two-thirds of a cycle within 2cm of tissue. More importantly, it induces a far more rapid drop-off in magnitudes. Similar to the observations above, such differences mean that the interpretation of experimental results may require consideration of the role of structural damping.

Despite the progress described here, it remains of great interest to explicitly solve the cell problems for specified alveolar geometries. A particular case of interest is that where the unit cell is a dodecahedron. Such a polyhedron is ideal because real alveolar sacs have a similar shape, and dodecahedra are nearly space filling and have suitable properties of periodicity [19]. In fact, previous work on the purely elastic properties of such polyhedra may be applicable [19]. Although the lung wall is isotropic, local structure can make the macroscopic properties anisotropic. An extension of the above would be to consider how anisotropies in the cell structure translate to anisotropies in the macroscopic behavior. If the primary load bearing elements of a dodecahedral alveolus are in the edges, but some faces allow more fluid flow than others, we may find a situation where the viscoelastic properties of the tissue in the absence of fluid flow are isotropic, whereas the pressure driven flow is biased by anisotropies in the permeability tensor. It will be of fundamental importance to compare "homogenized" behavior with experimental and computational results wherever possible. Explicit solution of the cell problems would give theoretical estimates for the parameters governing macroscopic lung behavior. For example, the Young's modulus of the lung would be estimated, and this could be compared with experimental measurements and also estimates based on different theoretical approaches.

Surfactant is increasingly recognized as being of fundamental importance in lung physiology. It allows the airways and alveoli to stay open at pressures which would not normally be adequate. The behavior of surfactant is quite nonlinear, depends on its history, and would seem to be hard to fit into the model framework described in this paper. However, in the regime of small-amplitude, high-frequency perturbations, it may be that surfactant simply alters the effective material parameters. Also, we have not attempted to deal with the considerable problems posed by trying to model oxygen and carbon dioxide levels in the lung, and their exchange at the alveolar surface. The inclusion of such highly nonlinear interactions presents an exciting challenge for future research.

One possible approach to simulating ventilation of the whole lung is to specify macroscopic coefficients according to their location within a region corresponding to the whole lung. Close to the "trachea" we would specify high permeability, but little elastic deformation, with a high degree of anisotropy to bias the flow down a "tube." With increasing distance one could allow increased elastic deformation, and more isotropic permeability to fluid flow.

Another approach is to use the immersed boundary method to simulate air flow in the large airways or bronchioles, and combine this with regions which obey the homogenized equations. Thus we would solve the Navier–Stokes equations in certain regions of a domain, coupled via appropriate boundary conditions to regions where the flow and deformation obeys the homogenized equations. We note that a number of the tools necessary to do this are available [9]. The immersed boundary method has been used extensively in the study of blood flow in the heart [23] and in blood vessels [10]. It allows the simulation of the flow of fluids and their interaction with

immersed elastic objects. Clearly the flow will stretch and distort such objects, which themselves exert a force on the fluid in response to their deformation. An additional strength of the immersed boundary method is the ease with which it can cope with complex geometries, such as are seen in the lung. In future work we intend to apply this technique to couple flows in the main airways to those in the respiratory tissue, with properties determined using the techniques described in this paper.

Appendix A. Homogenization details.

Here we describe the derivation of macroscopic equations from the dimensionless governing equations (2.17)–(2.21). The derivation is related to that by Burridge and Keller [2] and Lévy [20] for a purely elastic solid. We provide extensive details for this viscoelastic case, since we found the existing literature to be rather brief. Mathematically we consider the system variables as functions of independent variables $\mathbf{x}$ and $\mathbf{y}$, where $\mathbf{y} = \varepsilon^{-1}\mathbf{x}$. Here the crucial assumption is that variations on the small scale (i.e., with $\mathbf{y}$) are independent from those on the large scale $\mathbf{x}$ and thus we treat $\mathbf{x}$ and $\mathbf{y}$ as independent variables so that

$$\nabla f(\mathbf{x},\mathbf{y}) = \nabla f(\mathbf{x},\varepsilon^{-1}\mathbf{x}) = \nabla_{\mathbf{x}} f + \varepsilon^{-1}\nabla_{\mathbf{y}} f. \tag{A.1}$$

When considering ventilation of the lung we look for time-harmonic solutions (i.e., solutions proportional to $\exp(i\omega t) = \exp(it^*)$).

The second step in the homogenization process is to seek solutions to (2.17)–(2.21) which are asymptotic power series in ε. For example, the form for the fluid velocity would be

$$\mathbf{v}(\mathbf{x},\mathbf{y},\varepsilon) = \mathbf{v}^0(\mathbf{x},\mathbf{y}) + \varepsilon\mathbf{v}^1(\mathbf{x},\mathbf{y}) + \varepsilon^2\mathbf{v}_2(\mathbf{x},\mathbf{y}) + \mathcal{O}(\epsilon^3). \tag{A.2}$$

Similar expansions for the pressure p and the material displacement $\mathbf{u}$ and substitution of these series into (2.17)–(2.21) yield a system of linear equations for each successive order of ε.

Applying the assumptions of independent length scales and time harmonic solutions to the solid stress tensor $\underline{\underline{\mathcal{T}}}$, and the strain tensor $\underline{\underline{e}}$, it is clear that they will consist of terms of different orders in ε. Thus, we define the following quantities to aid in the correct decomposition of each term of the full governing equations into power series in ε:

$$\underline{\underline{e}}^n_{\xi} = \frac{\nabla_\xi \mathbf{u}^n + (\nabla_\xi \mathbf{u}^n)^T}{2} \quad \text{for} \quad \xi = \mathbf{x},\mathbf{y}, \quad n = 0,1,2,\ldots, \tag{A.3}$$

and

$$\underline{\underline{\mathcal{T}}}^n_{\xi} = \left(\frac{2E}{3} + i\mu_1\right)\underline{\underline{e}}^n_{\xi} \quad \text{for} \quad \xi = \mathbf{x},\mathbf{y}, \quad n = 0,1,2,\ldots. \tag{A.4}$$

So, for example, it follows from (A.1) that

$$\underline{\underline{e}} = \varepsilon^{-1}(\underline{\underline{e}}^0_{\mathbf{y}}) + (\underline{\underline{e}}^0_{\mathbf{x}} + \underline{\underline{e}}^1_{\mathbf{y}}) + \varepsilon(\underline{\underline{e}}^1_{\mathbf{x}} + \underline{\underline{e}}^2_{\mathbf{y}}) + \varepsilon^2(\underline{\underline{e}}^2_{\mathbf{x}} + \underline{\underline{e}}^3_{\mathbf{y}}) + \cdots, \tag{A.5}$$

$$\underline{\underline{\mathcal{T}}} = \varepsilon^{-1}(\underline{\underline{\mathcal{T}}}^0_{\mathbf{y}}) + (\underline{\underline{\mathcal{T}}}^0_{\mathbf{x}} + \underline{\underline{\mathcal{T}}}^1_{\mathbf{y}}) + \varepsilon(\underline{\underline{\mathcal{T}}}^1_{\mathbf{x}} + \underline{\underline{\mathcal{T}}}^2_{\mathbf{y}}) + \varepsilon^2(\underline{\underline{\mathcal{T}}}^2_{\mathbf{x}} + \underline{\underline{\mathcal{T}}}^3_{\mathbf{y}}) + \cdots \tag{A.6}$$

and, furthermore, that

$$\begin{aligned}\nabla\cdot\underline{\underline{\mathcal{T}}} &= \nabla_{\mathbf{x}}\cdot\underline{\underline{\mathcal{T}}} + \varepsilon^{-1}\nabla_{\mathbf{y}}\cdot\underline{\underline{\mathcal{T}}}\\ &= \varepsilon^{-2}(\nabla_{\mathbf{y}}\cdot\underline{\underline{\mathcal{T}^0_{\mathbf{y}}}}) + \varepsilon^{-1}(\nabla_{\mathbf{x}}\cdot\underline{\underline{\mathcal{T}^0_{\mathbf{y}}}} + \nabla_{\mathbf{y}}\cdot\underline{\underline{\mathcal{T}^0_{\mathbf{x}}}} + \nabla_{\mathbf{y}}\cdot\underline{\underline{\mathcal{T}^1_{\mathbf{y}}}})\\ &\quad +(\nabla_{\mathbf{x}}\cdot\underline{\underline{\mathcal{T}^0_{\mathbf{x}}}} + \nabla_{\mathbf{x}}\cdot\underline{\underline{\mathcal{T}^1_{\mathbf{y}}}} + \nabla_{\mathbf{y}}\cdot\underline{\underline{\mathcal{T}^1_{\mathbf{x}}}} + \nabla_{\mathbf{y}}\cdot\underline{\underline{\mathcal{T}^2_{\mathbf{y}}}})\\ &\quad +\varepsilon(\nabla_{\mathbf{x}}\cdot\underline{\underline{\mathcal{T}^1_{\mathbf{x}}}} + \nabla_{\mathbf{x}}\cdot\underline{\underline{\mathcal{T}^2_{\mathbf{y}}}} + \nabla_{\mathbf{y}}\cdot\underline{\underline{\mathcal{T}^2_{\mathbf{x}}}} + \nabla_{\mathbf{y}}\cdot\underline{\underline{\mathcal{T}^3_{\mathbf{y}}}}) + \cdots.\end{aligned} \tag{A.7}$$

(In general, take the superscript numeral and subtract the number of $\mathbf{y}$'s to get the appropriate power of ε.) (2.17)–(2.21) then yields, to order ε^0,

$$\nabla_{\mathbf{y}}p^0 = 0 \ \text{ in } \ D_f, \tag{A.8}$$

$$\nabla_{\mathbf{y}}\cdot\mathbf{v}^0 = 0 \ \text{ in } \ D_f, \tag{A.9}$$

$$\mathbf{v}^0 = i\mathbf{u}^0 \ \text{ on } \ \partial D_f = \partial D_s, \tag{A.10}$$

$$\mathbf{n}\cdot\underline{\underline{\mathcal{T}^0_{\mathbf{y}}}} = 0 \ \text{ on } \ \partial D_f = \partial D_s, \tag{A.11}$$

$$\nabla_{\mathbf{y}}\cdot\underline{\underline{\mathcal{T}^0_{\mathbf{y}}}} = 0 \ \text{ in } \ D_s; \tag{A.12}$$

and to order ε^1, we have

$$\nabla_{\mathbf{y}}p^1 - \mu\nabla^2_{\mathbf{y}}\mathbf{v}^0 + \nabla_{\mathbf{x}}p^0 + i\rho\mathbf{v}^0 = 0 \ \text{ in } \ D_f, \tag{A.13}$$

$$\nabla_{\mathbf{y}}\cdot\mathbf{v}^1 + \nabla_{\mathbf{x}}\cdot\mathbf{v}^0 = 0 \ \text{ in } \ D_f, \tag{A.14}$$

$$\mathbf{v}^1 = i\mathbf{u}^1 \ \text{ on } \ \partial D_f = \partial D_s, \tag{A.15}$$

$$\mathbf{n}\cdot(\underline{\underline{\mathcal{T}^1_{\mathbf{y}}}} + \underline{\underline{\mathcal{T}^0_{\mathbf{x}}}} + p^0\underline{\underline{I}}) = 0 \ \text{ on } \ \partial D_f = \partial D_s, \tag{A.16}$$

$$\nabla_{\mathbf{y}}\cdot\underline{\underline{\mathcal{T}^1_{\mathbf{y}}}} + \nabla_{\mathbf{y}}\cdot\underline{\underline{\mathcal{T}^0_{\mathbf{x}}}} + \nabla_{\mathbf{x}}\cdot\underline{\underline{\mathcal{T}^0_{\mathbf{y}}}} = 0 \ \text{ in } \ D_s. \tag{A.17}$$

A.1. p^0 and $\mathbf{u}^0$ are independent of $\mathbf{y}$. From (A.8) it follows that p^0 is independent of $\mathbf{y}$, so that

$$p^0 = p^0(\mathbf{x}) \quad \text{in} \quad D_f. \tag{A.18}$$

Now consider (A.12) and (A.11), which written in full give

$$\nabla_{\mathbf{y}}\cdot\left\{\left(\frac{2E}{3} + i\mu_1\right)\frac{\nabla_{\mathbf{y}}\mathbf{u}^0 + (\nabla_{\mathbf{y}}\mathbf{u}^0)^T}{2}\right\} = 0 \ \text{ in } \ D_s, \tag{A.19}$$

$$\mathbf{n}\cdot\left\{\left(\frac{2E}{3} + i\mu_1\right)\frac{\nabla_{\mathbf{y}}\mathbf{u}^0 + (\nabla_{\mathbf{y}}\mathbf{u}^0)^T}{2}\right\} = 0 \ \text{ on } \ \partial D_s. \tag{A.20}$$

Now let us take the dot product of the first equation with $\mathbf{u}^0$ and integrate over the solid domain D_s:

$$\left(\frac{2E}{3} + i\mu_1\right)\int_{D_s}\left(\nabla_{\mathbf{y}}\cdot\left\{\frac{\nabla_{\mathbf{y}}\mathbf{u}^0 + (\nabla_{\mathbf{y}}\mathbf{u}^0)^T}{2}\right\}\right)\cdot\mathbf{u}^0\ d\mathbf{y} = 0. \tag{A.21}$$

Then by the product rule

$$\int_{D_s} \nabla_{\mathbf{y}} \cdot \left(\left\{ \frac{\nabla_{\mathbf{y}}\mathbf{u}^0 + (\nabla_{\mathbf{y}}\mathbf{u}^0)^T}{2} \right\} \mathbf{u}^0 \right) d\mathbf{y} - \int_{D_s} \left\{ \frac{\nabla_{\mathbf{y}}\mathbf{u}^0 + (\nabla_{\mathbf{y}}\mathbf{u}^0)^T}{2} \right\} : (\nabla_{\mathbf{y}}\mathbf{u}^0)\, d\mathbf{y} = 0. \tag{A.22}$$

Note that $A : B$ indicates the matrix inner product of A and B (i.e., the sum of element-wise products). It can be seen that the first integral vanishes identically after applying the divergence theorem and using (A.20). Thus, by exploiting the symmetry of the strain tensor, we have

$$\int_{D_s} \left\{ \frac{\nabla_{\mathbf{y}}\mathbf{u}^0 + (\nabla_{\mathbf{y}}\mathbf{u}^0)^T}{2} \right\} : \left\{ \frac{\nabla_{\mathbf{y}}\mathbf{u}^0 + (\nabla_{\mathbf{y}}\mathbf{u}^0)^T}{2} \right\} = 0.$$

Hence $\{\nabla_{\mathbf{y}}\mathbf{u}^0 + (\nabla_{\mathbf{y}}\mathbf{u}^0)^T\}/2 = 0 \; \forall \; \mathbf{y} \in D_s$. Solutions to this equation are rigid body motions, and rotations are not bounded as a function of $\mathbf{y}$, so the only admissible solutions are translations, $\mathbf{u}^0$ constant. This translation may depend on $\mathbf{x}$, so we have

$$\mathbf{u}^0(\mathbf{x}, \mathbf{y}) = \mathbf{u}^0(\mathbf{x}) \quad \text{in} \quad D_s. \tag{A.23}$$

Thus p^0 and $\mathbf{u}^0$ are functions of $\mathbf{x}$ only.

A.2. Determination of $\mathbf{v^0}$. We introduce $\mathbf{w}$, the velocity of the fluid relative to the solid, defined by

$$\mathbf{v}^0(\mathbf{x}, \mathbf{y}) = \mathbf{w}(\mathbf{x}, \mathbf{y}) + i\mathbf{u}^0(\mathbf{x}) \quad \text{in} \quad D_f. \tag{A.24}$$

Then (A.9), (A.10), and (A.13) give the following set of inhomogeneous linear equations for $\mathbf{w}$ and p^1:

$$\nabla_{\mathbf{y}} \cdot \mathbf{w} = 0 \;\text{ in }\; D_f, \tag{A.25}$$

$$\nabla_{\mathbf{y}} p^1 - \mu \nabla_{\mathbf{y}}^2 \mathbf{w} + i\rho\mathbf{w} + \nabla_{\mathbf{x}} p^0 - \rho\mathbf{u}^0 = 0 \;\text{ in }\; D_f, \tag{A.26}$$

$$\mathbf{w} = 0 \;\text{ on }\; \partial D_f = \partial D_s. \tag{A.27}$$

The solutions to this problem are unique up to an additive scalar function of $\mathbf{x}$ in p^1 (since this would disappear upon taking its gradient). We therefore look for solutions which depend linearly on the inhomogeneous term $\nabla_{\mathbf{x}} p^0 - \rho\mathbf{u}^0$:

$$\mathbf{w}(\mathbf{x}, \mathbf{y}) = \underline{\underline{W}}(\mathbf{x}, \mathbf{y}) \{\nabla_{\mathbf{x}} p^0 - \rho\mathbf{u}^0\}, \tag{A.28}$$

$$p^1(\mathbf{x}, \mathbf{y}) = \mathbf{\Phi}(\mathbf{x}, \mathbf{y}) \cdot \{\nabla_{\mathbf{x}} p^0 - \rho\mathbf{u}^0\} + f(\mathbf{x}). \tag{A.29}$$

$\underline{\underline{W}}$ and $\mathbf{\Phi}$ are then determined as the solution to the corresponding *cell problem*:

$$\begin{aligned} \nabla_{\mathbf{y}} \cdot \underline{\underline{W}} &= 0 \quad \text{in} \quad D_f, \\ \nabla_{\mathbf{y}} \mathbf{\Phi} - \mu \nabla_{\mathbf{y}}^2 \underline{\underline{W}} + i\rho \underline{\underline{W}} + \underline{\underline{I}} &= 0 \quad \text{in} \quad D_f, \\ \underline{\underline{W}} &= 0 \quad \text{on} \quad \partial D_f = \partial D_s. \end{aligned} \tag{A.30}$$

Thus we have

$$\mathbf{v}^0(\mathbf{x}, \mathbf{y}) - i\mathbf{u}^0(\mathbf{x}) = \underline{\underline{W}}(\mathbf{x}, \mathbf{y}) \{\nabla_{\mathbf{x}} p^0(\mathbf{x}) - \rho\mathbf{u}^0(\mathbf{x})\}. \tag{A.31}$$

A.3. Determination of $\mathbf{u^1}$. Writing (A.17) and (A.16) in full and noting that the second and third terms in (A.17) are zero,

$$\nabla_{\mathbf{y}} \cdot \left(\left(\frac{2E}{3} + i\mu_1 \right) \frac{\nabla_{\mathbf{y}} \mathbf{u}^1 + (\nabla_{\mathbf{y}} \mathbf{u}^1)^T}{2} \right) = 0 \quad \text{in} \quad D_s, \tag{A.32}$$

$$\mathbf{n} \cdot \left(\left(\frac{2E}{3} + i\mu_1 \right) \left(\frac{\nabla_{\mathbf{y}} \mathbf{u}^1 + (\nabla_{\mathbf{y}} \mathbf{u}^1)^T}{2} + \frac{\nabla_{\mathbf{x}} \mathbf{u}^0 + (\nabla_{\mathbf{x}} \mathbf{u}^0)^T}{2} \right) + p^0 \underline{\underline{I}} \right) = 0 \quad \text{on} \quad \partial D_s. \tag{A.33}$$

Now we introduce the Hilbert space V of Ω-periodic vectors, defined in D_s, with $\int_{D_s} \mathbf{v} d\mathbf{y} = 0$ (so that $\mathbf{v}$ has zero mean value), and the scalar product

$$(\mathbf{u}, \mathbf{v})_V = \int_{D_s} \left(\frac{\nabla_{\mathbf{y}} \mathbf{u} + (\nabla_{\mathbf{y}} \mathbf{u})^T}{2} \right) : \left(\frac{\nabla_{\mathbf{y}} \bar{\mathbf{v}} + (\nabla_{\mathbf{y}} \bar{\mathbf{v}})^T}{2} \right) d\mathbf{y}. \tag{A.34}$$

Note that $\bar{\mathbf{v}}$ indicates the complex conjugate of $\mathbf{v}$.

Taking the dot product of (A.32) with $\bar{\mathbf{v}}$ and integrating over D_s with respect to $\mathbf{y}$,

$$\int_{D_s} \left(\nabla_{\mathbf{y}} \cdot \left(\left(\frac{2E}{3} + i\mu_1 \right) \frac{\nabla_{\mathbf{y}} \mathbf{u}^1 + (\nabla_{\mathbf{y}} \mathbf{u}^1)^T}{2} \right) \right) \cdot \bar{\mathbf{v}} d\mathbf{y} = 0, \tag{A.35}$$

and it follows from the product rule that

$$\begin{aligned} &\int_{D_s} \nabla_{\mathbf{y}} \cdot \left(\left(\frac{2E}{3} + i\mu_1 \right) \frac{\nabla_{\mathbf{y}} \mathbf{u}^1 + (\nabla_{\mathbf{y}} \mathbf{u}^1)^T}{2} \bar{\mathbf{v}} \right) d\mathbf{y} \\ &\qquad - \int_{D_s} \left(\left(\frac{2E}{3} + i\mu_1 \right) \frac{\nabla_{\mathbf{y}} \mathbf{u}^1 + (\nabla_{\mathbf{y}} \mathbf{u}^1)^T}{2} \right) : (\nabla_{\mathbf{y}} \bar{\mathbf{v}}) d\mathbf{y} = 0. \end{aligned} \tag{A.36}$$

We treat the first term of (A.36) by applying the divergence theorem and using (A.33), which applies on the boundary of the solid region:

$$\begin{aligned} &\int_{D_s} \nabla_{\mathbf{y}} \cdot \left(\left(\frac{2E}{3} + i\mu_1 \right) \frac{\nabla_{\mathbf{y}} \mathbf{u}^1 + (\nabla_{\mathbf{y}} \mathbf{u}^1)^T}{2} \bar{\mathbf{v}} \right) d\mathbf{y} \\ &\qquad = \int_{\partial D_s} \mathbf{n} \cdot \left(\left(\frac{2E}{3} + i\mu_1 \right) \frac{\nabla_{\mathbf{y}} \mathbf{u}^1 + (\nabla_{\mathbf{y}} \mathbf{u}^1)^T}{2} \bar{\mathbf{v}} \right) d\mathbf{y} \\ &\qquad = - \int_{\partial D_s} \mathbf{n} \cdot \left\{ \left(\left(\frac{2E}{3} + i\mu_1 \right) \frac{\nabla_{\mathbf{x}} \mathbf{u}^0 + (\nabla_{\mathbf{x}} \mathbf{u}^0)^T}{2} + p^0 \underline{\underline{I}} \right) \bar{\mathbf{v}} \right\} d\mathbf{y} \\ &\qquad = - \int_{\partial D_s} \mathbf{n} \cdot (\underline{\underline{A}} \bar{\mathbf{v}}) d\mathbf{y} \\ &\qquad = - \int_{\partial D_s} (\underline{\underline{A}} \mathbf{n}) \cdot \bar{\mathbf{v}} d\mathbf{y}, \end{aligned} \tag{A.37}$$

where the last step follows from the symmetry of $\underline{\underline{A}}$, the matrix of the inhomogeneous terms in (A.32) and (A.33):

$$\underline{\underline{A}} = \left(\frac{2E}{3} + i\mu_1 \right) \frac{\nabla_{\mathbf{x}} \mathbf{u}^0 + (\nabla_{\mathbf{x}} \mathbf{u}^0)^T}{2} + p^0 \underline{\underline{I}}. \tag{A.38}$$

By the symmetry of the strain and strain-rate tensors, the second term of (A.36) is just a constant times the scalar product:

$$\begin{aligned} &-\int_{D_s}\left(\left(\frac{2E}{3}+i\mu_1\right)\frac{\nabla_{\mathbf{y}}\mathbf{u}^1+(\nabla_{\mathbf{y}}\mathbf{u}^1)^T}{2}\right):(\nabla_{\mathbf{y}}\bar{\mathbf{v}})d\mathbf{y}\\ &\quad=-\left(\frac{2E}{3}+i\mu_1\right)\int_{D_s}\left(\frac{\nabla_{\mathbf{y}}\mathbf{u}^1+(\nabla_{\mathbf{y}}\mathbf{u}^1)^T}{2}\right):\left(\frac{\nabla_{\mathbf{y}}\bar{\mathbf{v}}+(\nabla_{\mathbf{y}}\bar{\mathbf{v}})^T}{2}\right)d\mathbf{y}\\ &\quad=-\left(\frac{2E}{3}+i\mu_1\right)(\mathbf{u}^1,\mathbf{v})_V, \end{aligned} \tag{A.39}$$

so that (A.36) becomes

$$-\int_{\partial D_s}(\underline{\underline{A}}\mathbf{n})\cdot\bar{\mathbf{v}}d\mathbf{y}-\left(\frac{2E}{3}+i\mu_1\right)(\mathbf{u}^1,\mathbf{v})_V=0, \tag{A.40}$$

and hence the variational form of the original problem may be written as

$$\left(\frac{2E}{3}+i\mu_1\right)(\mathbf{u}^1,\mathbf{v})_V=-\int_{\partial D_s}(\underline{\underline{A}}\mathbf{n})\cdot\bar{\mathbf{v}}d\mathbf{y}\quad\forall\mathbf{v}\in V. \tag{A.41}$$

The left-hand side is simply a complex constant times the scalar product defined above, and by the trace theorem, the right-hand side is a continuous form on V, which is clearly antilinear, so that by the Lax–Milgram theorem [24] there exists a unique solution $\mathbf{u}^1\in V$ to the above variational problem. The only restriction that we have placed on $\mathbf{u}^1$ in developing the variational formulation is that it has zero mean value, but this just means that the solution is unique up to the addition of a constant term (i.e., some function of $\mathbf{x}$). In our derivation of equations governing macroscopic averaged variables, we will require information only on $\nabla_{\mathbf{y}}\mathbf{u}^1$, which is uniquely determined. At this point it is interesting to note that this in turn specifies $\underline{\underline{\mathcal{T}^1_{\mathbf{y}}}}$, which corresponds to an order ε^0 stress in the macroscopic equations, itself due to an order ε^1 strain. The above uniqueness argument extends to this quantity.

It is important to remember that we require solutions for $\mathbf{u}^1$ to be $\mathbf{y}$-periodic, so that the seemingly obvious solution $\underline{\underline{\mathcal{T}^1_{\mathbf{y}}}}=-\underline{\underline{\mathcal{T}^0_{\mathbf{x}}}}-p^0\underline{\underline{I}}$ is in fact inadmissible. In order to determine the unique admissible solution, we look for one which depends linearly on the inhomogeneous terms, $\underline{\underline{A}}$. Thus we look for solutions of the form

$$u^1_i=\left(\frac{2E}{3}+i\mu_1\right)^{-1}Q_{ikl}A_{kl}, \tag{A.42}$$

where

$$A_{kl}=\left(\frac{2E}{3}+i\mu_1\right)\frac{1}{2}\left(\frac{\partial u^0_l}{\partial x_k}+\frac{\partial u^0_k}{\partial x_l}\right)+p^0\delta_{kl}. \tag{A.43}$$

We use index notation, whereby we sum over repeated indices—$Q_{ikl}(\mathbf{y})$ is a third rank tensor, because each component of the solution u^1 can depend on each element of A_{kl}. We have included the scaling of $(2E/3+i\mu_1)^{-1}$ to simplify the calculations that follow. Substituting this form for the solution and equating coefficients in A_{kl} give cell problems which determine Q_{ikl} and hence u^1_i.

Recall that we are seeking solutions to (A.32) and (A.33), which we rewrite in index notation:

$$\begin{aligned} \frac{\partial}{\partial y_j}\left\{\left(\frac{2E}{3}+i\mu_1\right)\left(\frac{\partial u_j^1}{\partial y_i}+\frac{\partial u_i^1}{\partial y_j}\right)\right\} &= 0 \quad \text{in} \quad D_s, \\ n_j\left\{\left(\frac{2E}{3}+i\mu_1\right)\left(\frac{\partial u_j^1}{\partial y_i}+\frac{\partial u_i^1}{\partial y_j}+\right)+2A_{ij}\right\} &= 0 \quad \text{on} \quad \partial D_s. \end{aligned} \tag{A.44}$$

Substitution of the proposed solution gives

$$\begin{aligned} \frac{\partial}{\partial y_j}\left\{\frac{\partial}{\partial y_i}\left(Q_{jkl}A_{kl}\right)+\frac{\partial}{\partial y_j}\left(Q_{ikl}A_{kl}\right)\right\} &= 0 \quad \text{in} \quad D_s, \\ n_j\left\{\frac{\partial}{\partial y_i}\left(Q_{jkl}A_{kl}\right)+\frac{\partial}{\partial y_j}\left(Q_{ikl}A_{kl}\right)+2\delta_{ik}\delta_{jl}A_{kl}\right\} &= 0 \quad \text{on} \quad \partial D_s, \end{aligned} \tag{A.45}$$

where the tensor $\delta_{ik}\delta_{jl}$ is the identity operator on 2×2 matrices. Notice that this gives the factor A_{kl} in each term, which is independent of y_i, and so we can interchange the order of multiplication and differentiation and factorize:

$$\begin{aligned} \frac{\partial}{\partial y_j}\left\{\frac{\partial Q_{jkl}}{\partial y_i}+\frac{\partial Q_{ikl}}{\partial y_j}\right\}A_{kl} &= 0 \quad \text{in} \quad D_s, \\ n_j\left\{\frac{\partial Q_{jkl}}{\partial y_i}+\frac{\partial Q_{ikl}}{\partial y_j}+2\delta_{ik}\delta_{jl}\right\}A_{kl} &= 0 \quad \text{on} \quad \partial D_s. \end{aligned} \tag{A.46}$$

The form of the cell problem for the 3-tensor Q_{ikl} is then

$$\begin{aligned} \frac{\partial}{\partial y_j}\left\{\frac{\partial Q_{jkl}}{\partial y_i}+\frac{\partial Q_{ikl}}{\partial y_j}\right\} &= 0 \quad \text{in} \quad D_s, \\ n_j\left\{\frac{\partial Q_{jkl}}{\partial y_i}+\frac{\partial Q_{ikl}}{\partial y_j}+2\delta_{ik}\delta_{jl}\right\} &= 0 \quad \text{on} \quad \partial D_s. \end{aligned} \tag{A.47}$$

We need only to find $n(n+1)/2$ entries of Q_{ikl} (where n is the number of spatial dimensions), since the symmetry of the strain tensor, and of A_{kl}, means that $Q_{ikl} = Q_{ilk}$.

All this calculation leads us to a form for the contribution of the order ε^1 displacement to the order ε^0 stress in the solid:

$$\underline{\underline{\mathcal{T}}}_{\mathbf{y}}^1 = \frac{\nabla_{\mathbf{y}}\underline{\underline{Q}}+(\nabla_{\mathbf{y}}\underline{\underline{Q}})^T}{2}\left(\left(\frac{2E}{3}+i\mu_1\right)\frac{\nabla_{\mathbf{x}}\mathbf{u}^0+(\nabla_{\mathbf{x}}\mathbf{u}^0)^T}{2}+p^0\underline{\underline{I}}\right). \tag{A.48}$$

A.4. Averaging and the derivation of macroscopic equations. We define the volume average of a quantity as

$$\langle f\rangle = \frac{1}{|\Omega|}\int_{\Omega_\eta} f\,d\mathbf{y}, \tag{A.49}$$

where Ω is the unit cell and Ω_η is that part of the cell over which f is defined.

A.4.1. Pressure driven flow. Equation (A.31) describes the flow through the solid, driven by the pressure gradient—it applies to the fluid domain, so that $\Omega_\eta = \Omega_f$, and averaging gives

$$\frac{1}{|\Omega|}\int_{\Omega_f}\mathbf{v}^0(\mathbf{x},\mathbf{y})d\mathbf{y} - \frac{1}{|\Omega|}\int_{\Omega_f} i\mathbf{u}^0(\mathbf{x})d\mathbf{y} = \frac{1}{|\Omega|}\int_{\Omega_f}\underline{\underline{W}}(\mathbf{x},\mathbf{y})\{\nabla_{\mathbf{x}}p^0(\mathbf{x}) - \rho\mathbf{u}^0(\mathbf{x})\}d\mathbf{y}. \tag{A.50}$$

Because $\mathbf{u}^0$ does not depend on $\mathbf{y}$, the second term is

$$\frac{1}{|\Omega|}\int_{\Omega_f} i\mathbf{u}^0(\mathbf{x})d\mathbf{y} = i\mathbf{u}^0(\mathbf{x})\frac{1}{|\Omega|}\int_{\Omega_f} d\mathbf{y} = i\mathbf{u}^0(\mathbf{x})\frac{|\Omega_f|}{|\Omega|}, \tag{A.51}$$

which leads us to introduce the porosity $\phi = \frac{|\Omega_f|}{|\Omega|}$. p^0 also does not depend on $\mathbf{y}$, and so we have

$$\langle\mathbf{v}^0\rangle(\mathbf{x}) - i\frac{|\Omega_f|}{|\Omega|}\mathbf{u}^0(\mathbf{x}) = \langle\underline{\underline{W}}\rangle(\mathbf{x})\{\nabla_{\mathbf{x}}p^0(\mathbf{x}) - \rho\mathbf{u}^0(\mathbf{x})\}. \tag{A.52}$$

A.4.2. Mass conservation. Using the fact that $\mathbf{v}^1 = i\mathbf{u}^1$ on $\partial D_f = \partial D_s$ (equation (A.15)), the divergence theorem, and noting that outward pointing normals for the fluid and solid part point in opposite directions:

$$\begin{aligned}\langle\nabla_{\mathbf{y}}\cdot\mathbf{v}^1\rangle &= \frac{1}{|\Omega|}\int_{\Omega_f}\nabla_{\mathbf{y}}\cdot\mathbf{v}^1 d\mathbf{y},\\ &= \frac{1}{|\Omega|}\int_{\partial\Omega_f}\mathbf{n}\cdot\mathbf{v}^1 d\mathbf{y},\\ &= \frac{i}{|\Omega|}\int_{\partial\Omega_s}\mathbf{n}\cdot\mathbf{u}^1 d\mathbf{y},\\ &= -\frac{i}{|\Omega|}\int_{\Omega_s}\nabla_{\mathbf{y}}\cdot\mathbf{u}^1 d\mathbf{y},\\ &= -i\langle\nabla_{\mathbf{y}}\cdot\mathbf{u}^1\rangle.\end{aligned} \tag{A.53}$$

The key step now is to average (A.14):

$$\begin{aligned}&\langle\nabla_{\mathbf{x}}\cdot\mathbf{v}^0\rangle + \langle\nabla_{\mathbf{y}}\cdot\mathbf{v}^1\rangle = 0\\ \Rightarrow\quad &\langle\nabla_{\mathbf{x}}\cdot\mathbf{v}^0\rangle - i\langle\nabla_{\mathbf{y}}\cdot\mathbf{u}^1\rangle = 0\\ \Rightarrow\quad &\nabla_{\mathbf{x}}\cdot\langle\mathbf{v}^0\rangle - i\left\langle\left(\frac{2E}{3}+i\mu_1\right)^{-1}\left(\nabla_{\mathbf{y}}\cdot\underline{\underline{\underline{\underline{Q}}}}(\mathbf{y})\right) : \underline{\underline{A}}\right\rangle = 0\\ \Rightarrow\ &\nabla_{\mathbf{x}}\cdot\langle\mathbf{v}^0\rangle - i\left\langle\nabla_{\mathbf{y}}\cdot\underline{\underline{\underline{\underline{Q}}}}(\mathbf{y})\right\rangle : \left(\frac{\nabla_{\mathbf{x}}\mathbf{u}^0 + (\nabla_{\mathbf{x}}\mathbf{u}^0)^T}{2} + \left(\frac{2E}{3}+i\mu_1\right)^{-1}p^0\underline{\underline{I}}\right) = 0.\end{aligned} \tag{A.54}$$

A.4.3. Balance of momentum. Finally, we derive a balance of momentum equation, using the fact that the total momentum due to the fluid and solid acceleration must equal the divergence of the total stress, at first order:

$$i\rho\langle\mathbf{v}^0\rangle - \mathbf{u}^0 = \nabla_{\mathbf{x}}\cdot\langle(\underline{\underline{\mathcal{T}_{\mathbf{y}}}}^1 + \underline{\underline{\mathcal{T}_{\mathbf{x}}}}^0)\rangle - \nabla_{\mathbf{x}}\cdot(\phi p^0\underline{\underline{I}}), \tag{A.55}$$

so that

$$i\rho\langle \mathbf{v}^0\rangle - \mathbf{u}^0 = \nabla_{\mathbf{x}}\cdot\left\{\left(\frac{2E}{3}+i\mu_1\right)\left\langle \frac{\nabla_{\mathbf{y}}\underline{\underline{Q}}+(\nabla_{\mathbf{y}}\underline{\underline{Q}})^T}{2}+\underline{\underline{I}}\right\rangle \frac{\nabla_{\mathbf{x}}\mathbf{u}^0+(\nabla_{\mathbf{x}}\mathbf{u}^0)^T}{2}\right\}$$

$$+\left(\left\langle \frac{\nabla_{\mathbf{y}}\underline{\underline{Q}}+(\nabla_{\mathbf{y}}\underline{\underline{Q}})^T}{2}\underline{\underline{I}}\right\rangle - \phi\underline{\underline{I}}\right)\nabla_{\mathbf{x}}\cdot(p^0\underline{\underline{I}}). \tag{A.56}$$

Note that here the fluid stress is averaged over the fluid domain and the solid stress is averaged over the solid domain.

A.4.4. Macroscopic equations. Collecting these results together, we get the following equations for the mean quantities $\mathbf{V}, P, \mathbf{U}$, whose dependence on the macroscopic spatial scale, $\mathbf{x}$, is implicit:

$$\begin{aligned}\mathbf{V}-i\phi\mathbf{U} &= -\underline{\underline{K}}\left(\nabla P-\rho\mathbf{U}\right),\\ \nabla\cdot(\mathbf{V}-i\phi\mathbf{U}) &= i\left(\underline{\underline{\alpha}}:\tfrac{\nabla\mathbf{U}+(\nabla\mathbf{U})^T}{2}+\beta P\right),\\ i\rho\mathbf{V}-\mathbf{U} &= \nabla\cdot\left(\underline{\underline{C}}\tfrac{\nabla\mathbf{U}+(\nabla\mathbf{U})^T}{2}+\underline{\underline{\alpha}}P\right).\end{aligned} \tag{A.57}$$

The parameters for this system are given by

$$\underline{\underline{K}} = -\langle\underline{\underline{W}}(\mathbf{y})\rangle = \frac{1}{|\Omega|}\int_{\Omega_f}\underline{\underline{W}}(\mathbf{y})d\mathbf{y}, \tag{A.58}$$

$$\underline{\underline{\alpha}} = \langle\nabla_{\mathbf{y}}\cdot\underline{\underline{Q}}\rangle - \phi\underline{\underline{I}}, \tag{A.59}$$

$$\beta = \left(\frac{2E}{3}+i\mu_1\right)^{-1}\mathrm{Trace}(\langle\nabla_{\mathbf{y}}\cdot\underline{\underline{\mathrm{Q}}}\rangle), \tag{A.60}$$

and

$$\underline{\underline{C}} = \left(\frac{2E}{3}+i\mu_1\right)\left(\left\langle\frac{\nabla_{\mathbf{y}}\underline{\underline{Q}}+(\nabla_{\mathbf{y}}\underline{\underline{Q}})^T}{2}\right\rangle+(1-\phi)\underline{\underline{I}}\right). \tag{A.61}$$

This completes the derivation of the macroscopic equations.

Appendix B. Assumption of macroscopic isotropy. Here we show how, if we assume the macrosopic properties of lung tissue are isotropic, we may estimate all the tissue parameters given experimental measurements of Young's modulus and Poisson ratio. For isotropic lung tissue, tensors become scalars, and the macroscopic equations are

$$\mathbf{V}-i\phi\mathbf{U} = -K\left(\nabla P-\rho\mathbf{U}\right), \tag{B.1}$$

$$\nabla\cdot(\mathbf{V}-i\phi\mathbf{U}) = i\left(\alpha\theta+\beta P\right), \tag{B.2}$$

$$i\rho\mathbf{V}-\mathbf{U} = \nabla\cdot\left\{\underline{\underline{\mathcal{T}}}+\alpha\underline{\underline{I}}P\right\}, \tag{B.3}$$

where the solid stress is now

$$\underline{\underline{\mathcal{T}}} = \underline{\underline{\underline{\underline{C}}}}\,\underline{\underline{e}} = \frac{\hat{E}}{1+\hat{\nu}}\left(\underline{\underline{e}} + \frac{\hat{\nu}}{1-2\hat{\nu}}\,\theta\underline{\underline{I}}\right) + i\hat{\mu}_1\,\underline{\underline{e}} + i\hat{\mu}_2\,\theta\underline{\underline{I}}. \tag{B.4}$$

$\underline{\underline{e}}$ and $\theta = \text{Trace}\,(\underline{\underline{e}})$ are the macroscopic strain tensor and dilation, respectively. $\hat{E}$ and $\hat{\nu}$ are the macroscopic Young's modulus and Poisson ratio, which have been experimentally measured and theoretically predicted for lung tissue [15, 16, 19]; $\hat{\mu}_1$ and $\hat{\mu}_2$ are macrosopic shear and bulk viscosities, which we will show can be expressed in terms of $\hat{E}, \hat{\nu}, E$, and μ_1—also enabling us to determine α and β. This is because we must be able to decompose C_{ijkl} into a linear combination of identity and trace operators on the space of 2×2 matrices. We begin by expressing this in index notation:

$$\begin{aligned} C_{ijkl} &= \left(\frac{2E}{3} + i\mu_1\right) a \overbrace{\delta_{ik}\delta_{jl}}^{\text{Identity}} + \left(\frac{2E}{3} + i\mu_1\right) b \overbrace{\delta_{ij}\delta_{kl}}^{\text{Trace}} \\ &= \left(\frac{\hat{E}}{1+\hat{\nu}} + i\hat{\mu}_1\right)\delta_{ik}\delta_{jl} + \left(\frac{\hat{E}}{1+\hat{\nu}}\frac{\hat{\nu}}{1-2\hat{\nu}} + i\hat{\mu}_2\right)\delta_{ij}\delta_{kl}. \end{aligned} \tag{B.5}$$

Taking the real parts, equating the coefficients of the identity and trace operators, and assuming that $E, \hat{E}$, and $\hat{\nu}$ are known give

$$a = \frac{\hat{E}}{1+\hat{\nu}}\,\frac{3}{2E}, \quad b = \frac{\hat{E}}{1+\hat{\nu}}\frac{\hat{\nu}}{1-2\hat{\nu}}\,\frac{3}{2E}. \tag{B.6}$$

Then similarly, by equating the imaginary parts and assuming that μ_1 is known, we must have

$$\hat{\mu}_1 = \mu_1 a = \mu_1 \frac{3\hat{E}}{2E(1+\hat{\nu})}, \quad \hat{\mu}_2 = \mu_1 b = \mu_1 \frac{3\hat{E}\hat{\nu}}{2E(1+\hat{\nu})(1-2\hat{\nu})}. \tag{B.7}$$

Now to find α and β we need information about $\langle \nabla_{\mathbf{y}} \cdot \underline{\underline{\underline{Q}}} \rangle$. From the definition of C_{ijkl} we know that

$$\begin{aligned} C_{ijkl} &= \left(\frac{2E}{3} + i\mu_1\right)(a\delta_{ik}\delta_{jl} + b\delta_{ij}\delta_{kl}) \\ &= \left(\frac{2E}{3} + i\mu_1\right)\left(\frac{1}{2}\left\langle \frac{\partial Q_{jkl}}{\partial y_i} + \frac{\partial Q_{ikl}}{\partial y_j}\right\rangle + (1-\phi)\delta_{ik}\delta_{jl}\right) \end{aligned} \tag{B.8}$$

and hence that

$$\frac{1}{2}\left\langle \frac{\partial Q_{jkl}}{\partial y_i} + \frac{\partial Q_{ikl}}{\partial y_j}\right\rangle = (a+\phi-1)\delta_{ik}\delta_{jl} + b\delta_{ij}\delta_{kl}. \tag{B.9}$$

So now we can calculate $\langle \nabla_{\mathbf{y}} \cdot \underline{\underline{\underline{Q}}} \rangle$, which will in turn give α and β:

$$\begin{aligned} \langle \nabla_{\mathbf{y}} \cdot \underline{\underline{\underline{Q}}} \rangle_{ij} &= \left\langle \frac{\partial Q_{kij}}{\partial y_k} \right\rangle \\ &= \frac{1}{2}\left\langle \frac{\partial Q_{kij}}{\partial y_k} + \frac{\partial Q_{kij}}{\partial y_k} \right\rangle \\ &= (a+\phi-1)\delta_{ki}\delta_{kj} + b\delta_{kk}\delta_{ij} \\ &= (a+\phi-1)\delta_{ij} + 3b\delta_{ij} \\ &= (a+3b+\phi-1)\delta_{ij}, \end{aligned} \tag{B.10}$$

so that

$$\alpha = a + 3b - 1 = \frac{3\hat{E}}{2E(1-2\hat{\nu})} - 1, \tag{B.11}$$

and

$$\begin{aligned}\beta &= \left(\frac{2E}{3} + i\mu_1\right)^{-1} \mathrm{Trace}(\langle \nabla_{\mathbf{y}} \cdot \underline{\underline{\mathrm{Q}}} \rangle) \\ &= \left(\frac{2E}{3} + i\mu_1\right)^{-1} 3(a + 3b + \phi - 1) \\ &= 3\left(\frac{2E}{3} + i\mu_1\right)^{-1} \left(\frac{3\hat{E}}{2E(1-2\hat{\nu})} + \phi - 1\right). \end{aligned} \tag{B.12}$$

This completes the derivation of all the tissue parameters in terms of those quantities for which we have reasonable estimates, namely the Young's modulus and shear viscosity of the alveolar wall, the Young's modulus and Poisson ratio of bulk lung tissue, and the lung porosity.

Appendix C. One dimensional system. We separate the one dimensional system of equations (5.1)–(5.3) into real and imaginary parts, noting that the permeability and elasticity tensor are now complex scalars, K and C; β is complex, and the other parameters, ρ, α, ϕ, are real numbers. We use the subscript r to denote the real part, and i for the imaginary part:

$$V_r + \phi U_i + K_r P_r' - K_r \rho U_r - K_i P_i' + K_i \rho U_i = 0, \tag{C.1}$$

$$V_i - \phi U_r + K_r P_i' - K_r \rho U_i + K_i P_r' - K_i \rho U_r = 0, \tag{C.2}$$

$$V_r' + (\phi + \alpha) U_i' + \beta_i P_r + \beta_r P_i = 0, \tag{C.3}$$

$$V_i' - (\phi + \alpha) U_r' - \beta_r P_r + \beta_i P_i = 0, \tag{C.4}$$

$$\rho V_i + U_r + C_r U_r'' - C_i U_i'' + \alpha P_r' = 0, \tag{C.5}$$

$$\rho V_r - U_i - C_i U_r'' - C_r U_i'' - \alpha P_i' = 0. \tag{C.6}$$

Writing $W_r = U_r'$ and $W_i = U_i'$, solving (C.1) and (C.2) for P_r' and P_i' in terms of V_r, V_i, U_r, U_i, substituting this into (C.5) and (C.6), and solving for W_r' and W_i' give

$$V_r' = -(\phi + \alpha) W_i - \beta_i P_r - \beta_r P_i, \tag{C.7}$$

$$V_i' = (\phi + \alpha) W_r + \beta_r P_r - \beta_i P_i, \tag{C.8}$$

$$U_r' = W_r, \tag{C.9}$$

$$U_i' = W_i, \tag{C.10}$$

$$\begin{aligned} W_r' = &\left(\alpha \frac{C_r K_i + C_i K_r}{|C|^2 |K|^2} - \frac{C_r \rho}{|C|^2}\right) V_r + \left(\alpha \frac{C_r K_r - C_i K_i}{|C|^2 |K|^2} + \frac{C_i \rho}{|C|^2}\right) V_i \\ &+ \left(\alpha\phi \frac{C_i K_i - C_r K_r}{|C|^2 |K|^2} + \frac{C_i \rho \alpha}{|C|^2} + \frac{C_i}{|C|^2}\right) U_r - \left(\alpha\phi \frac{C_r K_i + C_i K_r}{|C|^2 |K|^2} + \frac{C_r \rho \alpha}{|C|^2} + \frac{C_r}{|C|^2}\right) U_i, \end{aligned} \tag{C.11}$$

$$W_i' = \left(\alpha\frac{C_rK_r - C_iK_i}{|C|^2|K|^2} + \frac{C_i\rho}{|C|^2}\right)V_r + \left(\alpha\frac{C_rK_i + C_iK_r}{|C|^2|K|^2} - \frac{C_r\rho}{|C|^2}\right)V_i \tag{C.12}$$

$$- \left(\alpha\phi\frac{C_rK_i + C_iK_r}{|C|^2|K|^2} + \frac{C_r\rho\alpha}{|C|^2} + \frac{C_r}{|C|^2}\right)U_r - \left(\alpha\phi\frac{C_rK_r - C_iK_i}{|C|^2|K|^2} + \frac{C_i\rho\alpha}{|C|^2} + \frac{C_i}{|C|^2}\right)U_i,$$

$$P_r' = -\frac{K_r}{|K|^2}V_r - \frac{K_i}{|K|^2}V_i + \phi\frac{K_i}{|K|^2}U_r + \rho U_r - \phi\frac{K_r}{|K|^2}U_i, \tag{C.13}$$

$$P_i' = \frac{K_i}{|K|^2}V_r - \frac{K_r}{|K|^2}V_i + \phi\frac{K_r}{|K|^2}U_r + \rho U_i + \phi\frac{K_i}{|K|^2}U_i. \tag{C.14}$$

This is a system of eight ODEs, for which explicit solutions can be found.

Acknowledgments. We thank David Eyre, Aaron Fogelson, Jim Keener, and Steve Kern for a number of helpful discussions.

REFERENCES

[1] M. A. Biot, *Generalized theory of acoustic propagation in porous dissipative media*, J. Acoust. Soc. Am., 34 (1962), pp. 1254–1264.
[2] R. Burridge and J. B. Keller, *Poroelasticity equations derived from microstructure*, J. Acoust. Soc. Am., 70 (1981), pp. 1140–1146.
[3] H. K. Chang, *Mechanisms of gas transport during ventilation by high-frequency oscillation*, J. Appl. Physiol., 56 (1984), pp. 553–563.
[4] A. J. Chorin and J. E. Marsden, *A Mathematical Introduction to Fluid Mechanics*, Springer-Verlag, New York, 1992.
[5] R. H. Clark, D. R. Gerstmann, D. M. Null, B. A. Yoder, J. D. Cornish, C. M. Glasier, N. B. Ackerman, R. E. Bell, and R. A. Delemos, *Pulmonary interstitial emphysema treated by high-frequency oscillatory ventilation*, Crit. Care Med., 14 (1986), pp. 926–930.
[6] C. Darquenne and M. Paiva, *Two- and three-dimensional simulations of aerosol transport and deposition in alveolar zone of human lung*, J. Appl. Physiol., 80 (1996), pp. 1401–1414.
[7] B. L. K. Davey and J. H. T. Bates, *Regional lung impedance from forced oscillations through alveolar capsules*, Respir. Physiol., 91 (1993), pp. 165–182.
[8] E. Denny and R. C. Schroter, *The mechanical behavior of a mammalian lung alveolar duct model*, J. Biomech. Eng., 117 (1995), pp. 254–261.
[9] D. Eyre and A. Fogelson, *IBIS: A User's Guide*, University of Utah, Salt Lake City, 1997.
[10] A. L. Fogelson, *A mathematical model and numerical method for studying platelet adhesion and aggregation during blood clotting*, J. Comput. Phys., 56 (1984), pp. 111–134.
[11] J. J. Fredberg and A. Hoenig, *Mechanical response of the lungs at high frequencies*, J. Biomech. Eng., 100 (1977), pp. 57–66.
[12] J. J. Fredberg and J. A. Moore, *The distributed response of complex branching duct networks*, J. Acoust. Soc. Am., 63 (1978), pp. 954–961.
[13] J. J. Fredberg and D. Stamenovic, *On the imperfect elasticity of lung tissue*, J. Appl. Physiol., 67 (1989), pp. 2408–2419.
[14] H. Fukaya, C. Martin, A. Young, and S. Katsura, *Mechanical properties of alveolar walls*, J. Appl. Physiol., 25 (1968), pp. 689–695.
[15] Y. C. Fung, *Microrheology and constitutive equation of soft tissue*, Biorheology, 25 (1988), pp. 261–270.
[16] Y. C. Fung, *Connecting incremental shear modulus and Poisson's ratio of lung tissue with morphology and rheology of microstructure*, Biorheology, 26 (1989), pp. 279–289.
[17] K. C. High, J. S. Ultman, and S. R. Karl, *Mechanically induced pendelluft flow in a model airway bifurcation during high frequency oscillation*, J. Biomech. Eng., 113 (1991), pp. 342–347.
[18] K. Horsfield and G. Cummings, *Morphology of the bronchial tree in men*, J. Appl. Physiol., 24 (1968), pp. 373–383.
[19] E. Kimmel, R. D. Kamm, and A. H. Shapiro, *A cellular model of lung elasticity*, J. Biomech. Eng., 109 (1987), pp. 126–131.

[20] T. Lévy, *Propagation of waves in a fluid-saturated porous elastic solid*, Int. J. Eng. Sci., 17 (1979), pp. 1005–1014.
[21] A. I. Lur'e, *Three-Dimensional Problems of the Theory of Elasticity*, John Wiley, New York, 1964.
[22] A. B. Otis, C. B. McKerrow, R. A. Bartlett, J. Mead, M. B. McIlroy, N. J. Selverstone, and E. P. Radford, Jr., *Mechanical factors in distribution of pulmonary ventilation*, J. Appl. Physiol., 8 (1956), pp. 427–443.
[23] C. S. Peskin and D. M. McQueen, *Modeling prosthetic heart valves for numerical analysis of blood flow in the heart*, J. Comput. Phys., 37 (1980), pp. 113–132.
[24] E. Sanchez-Palencia, *Non-Homogenous Media and Vibration Theory*, Springer-Verlag, New York, 1980.